New Jersey Institute of Technology

Digital Commons @ NJIT

Spring 5-31-2017

Memorizing chromic response to pressure

Maulik Kiritkumar Padh
New Jersey Institute of Technology

Follow this and additional works at: https://digitalcommons.njit.edu/theses

Part of the Materials Science and Engineering Commons

Recommended Citation

ABSTRACT

MEMORIZING CHROMIC RESPONSE TO PRESSURE

by
Maulik Kiritkumar Padh

Almost all appliances are prone to mechanical stress in one form or the other. An increasing dependence on machines in daily life calls for a need to increase their maintenance quality. Various materials, methods and configurations to observe mechanical pressure have been devised and this paper discusses one such technique. The use of gold nanoparticles in its one dimensional array causes plasmonic coupling between the nanoparticles, which when disrupted creates a plasmonic shift in its assembly. Such a film, when casted on a polymer with a known elastic limit, causes deformation by an application of stress. This forces the film to undergo plasmonic shift permanently and this is sensed with a change in colour. Because of plastic deformation, the colour remains intact even after the removal of pressure. Analysis of extinction profiles of nanoparticles have been carried out which demonstrates the proof of concept under a wide range of stresses. The colour change depends on the duration of application of stress and the value of stress itself. This is one of the earliest attempts to develop a colorimetric pressure-responsive film which memorizes the colour change by using gold nanoparticles. In this thesis, an attempt is made to investigate the feasibility of using silver nanoparticles in such sensors.

MEMORIZING CHROMIC RESPONSE TO PRESSURE

by
Maulik Kiritkumar Padh

A Thesis
Submitted to the Faculty of
New Jersey Institute of Technology
in Partial Fulfilment of the Requirements for the Degree of
Master of Science in Materials Science and Engineering

Department of Applied Physics

May 2017

Blank Page

APPROVAL PAGE

MEMORIZING CHROMIC RESPONSE TO PRESSURE

Maulik Kiritkumar Padh

Dr. Nuggehalli M. Ravindra, Thesis Advisor	Date
Professor of Materials Science and Engineering, NJIT	

Dr. Michael Jaffe, Committee Member	Date
Research Professor of Biomedical Engineering, NJIT	

Dr. Sagnik Basuray, Committee Member	Date
Assistant Professor of Chemical, Biological and Pharmaceutical Engineering, NJIT	

BIOGRAPHICAL SKETCH

Author: Maulik Kiritkumar Padh

Degree: Master of Science

Date: May 2017

Undergraduate and Graduate Education:

- Master of Science in Materials Science and Engineering,
  New Jersey Institute of Technology, Newark, New Jersey, USA, 2017

- Master of Science in Physics,
  Maharaja Sayajirao University, Vadodara, Gujarat, India, 2015

- Bachelor of Science in Physics,
  Maharja Sayajirao University, Vadodara, Gujarat, India, 2013

Major: Materials Science and Engineering

ACKNOWLEDGEMENT

I would first like to thank my thesis advisor Dr. Nugehalli M. Ravindra (Ravi) of the Interdisciplinary Program in Materials Science & Engineering Program and Applied Physics Department at the New Jersey Institute of Technology. The door to Prof. Ravi's office is always open whenever I run into a trouble spot or have a question about my research or writing. He consistently allowed this Thesis to be my own work, but steered me in the right direction whenever I needed it.

I would also like to acknowledge the committee members Dr. Michael Jaffe of the Department of Biomedical Engineering at New Jersey Institute of Technology and Dr. Sagnik Basuray of the Department of Chemical, Biological and Pharmaceutical Engineering at New Jersey Institute of Technology for their very valuable comments on this thesis.

Finally, I must express my very profound gratitude to my parents for providing me with unfailing support and continuous encouragement throughout my years of study and through the process of researching and writing this thesis. This accomplishment would not have been possible without them.

TABLE OF CONTENTS

TABLE OF CONTENTS
(Continued)

LIST OF FIGURES

CHAPTER 1

INTRODUCTION

1.1 Role of Pressure Sensors

Pressure is a force that resists the external stimuli against deformation of the solid and is calculated as force per unit area. Depending on the amount of pressure applied, a signal is triggered in this sensor and therefore it can also be considered as a transducer. Type of signal is the key difference. Such a signal can be electrical, thermal, optical, magnetic, acoustic or simply a change in colour. Pressure sensors are of different types: Altitude pressure sensors which are useful in aircraft, satellites, weather, and barometric applications; To measure liquid flow, we use Flow sensors which are based on differential pressure measurements; Leak sensors are used to measure pressure decay.

This thesis focuses on the influence of pressure on solids. Typical pressure sensing applications range from common everyday uses and life support to exotic investigational devices. Devices addressing measurements such as friction, stretch and strain detection, collision with a surface and other such applications, benefit from advancing Mechanochromic sensor technology. Many technologies, for the purpose of manufacturing the pressure sensors, include semiconductor piezo resistive, strain gauge, microelectromechanical structures (MEMS), mechanical deflection, and vibrating capacitance.

This technology also exploits the mechanical properties of a liquid to measure its pressure. This property is the material's viscous flow, which is dependent on the duration of stress and its intensity. There will be a reaction to this stress, which will be detected by the colour change

1.2 Colorimetric Pressure Indicating Film

This pressure indicating film would be unique, affordable and easy-to-use tool that identifies the distribution, duration and magnitude of pressure between any two contacting or impacting surfaces. The best part of this pressure indicating sensor film is that the films are extremely thin (4 to 8 mils) which also helps in finding the stress of curved surfaces. Such films are an alternative to electronic transducers which are not useful in tight spaces and intolerant environments.

Technologies have started to greatly rely on the "Nano" world as they exhibit special property due to the structure and dimension, which is greatly different from the particles we call as bulk materials. The size of interest is usually from 1-1000 nm. They can absorb as well as scatter the light in different directions and in different conditions. It is because of this reason that we can observe colour change due to external stimulus. Special property of nanoparticles is that the properties differs greatly in terms of an individual particle and a group of such particles. The particles in close proximity starts interacting and if they are arranged in a fixed pattern, then the force of a particular form starts acting. The uniform force makes them act like a single unit and thus exhibit unique properties. This unit can be manipulated by handling their patterns, which will reveal their assembly and disassembly behaviour. The type units will help to form stimuli-responsive materials which are famously known as "Smart Materials". [49] [50]

The Gold nanoparticles used are approximately of size 15 nm. In this analysis, AuNPs are studied as a reference to understand the effect of external stimuli to the films, which are designed for the pressure sensing purpose. An attempt to understand the same effect, if the gold is replaced by silver nanoparticles, is carried out in this thesis.

1.3 Working Principle

It is the relationship between stress and irreversible viscous deformation that governs the principle of this film. The composite film is basically a casting of a homogeneous mixture of AuNP chains with polymer solution. The relationship makes use of Kelvin-Voigt model and Newton's law of viscosity which are explained afterwards. Using them will lead to the following equation:

$$\varepsilon(to) = \int_0^{t0} \frac{\sigma(t)}{\eta} dt \qquad (1.1)$$

where, extent of deformation, ε, is proportional to the intensity of the applied stress σ and duration time t_0 and is inversely proportional to the viscosity of the material η.

Pressing or stretching of the film results in an increasing inter-particle distance which weakens the Plasmon coupling. The shift in the position of the Plasmon band is related to the extent of film deformation for a given period and is proportional to the applied stress. This is how a film with a property of stress memory is produced which gives an output with a colour change. [51] [52]

The film is placed between any two surfaces that touch, mate or impact. When pressure is applied for a brief amount of time and removed, the film reveals the pressure pattern that occurs between the two surfaces for that specific duration of time. The intensity of colour on the film is directly related to the amount of pressure applied for a given period of time. It can be used in a bolted joint interface, composite layout, heat sealing and lamination or press, as a force sensing resistor. It has various measuring applicability such as surface pressure distribution in terms of an impact force sensor, seat pressure sensor, as a strain gauge or even as nip impression paper.

1.4 Surface Plasmon Resonance

In a subwavelength scale nanostructure, surface plasmon resonance is plasmonic in nature. Photons are the constituent particles of electromagnetic radiation. Thus, any travelling light consists of photons of a particular frequency and wavelength. The surface of metals consist of electrons which are oscillating against the restoring force. When the frequency of the incident light matches the natural frequency of these surface electrons, it gives rise to the resonance condition. In short, SPR is the conduction of electrons oscillating in its resonant frequency at the interface, stimulated by an incident light between the positive and negative permittivity material. It is considered to be the fundamental principle behind the bio-sensor applications which are colour based. LSPRs are localized surface plasmon resonances and represent oscillation of collection of electron charges in metallic nanoparticles, caused by the irradiation of an incident light. At resonance wavelength, the near-field amplitude is enhanced. Magneto-optical effects are also enhanced by LSPRs due to the enhanced near-field amplitude. [53] [54]

1.5 Plasmon Coupling

When the nanoparticles are arranged in close proximity, they will undergo LSPR. In case of AuNPs, this excitation of plasmon is controlled by arranging it in linear chains. Because of this formation, the nanoparticles would interact, resulting in the effect known as "Plasmon Coupling". By virtue of the separation between these particles, designing such pressure sensors are possible.

When an assembly of nanoparticles has been formed, there are usually two types of interactions that are common: Near-field and Far-field coupling. The difference is in the inter-particle distance with respect to the size of nanoparticles. If the distance is

much smaller than the NP size, then the dominating interaction is near-field coupling with d^{-3} dependence (d is the inter-particle size) because there is a short-range electromagnetic field interaction between adjacent nanoparticles of the range of tens of nanometres. The near and far field plasmon coupling can be changed by changing the inter-particle distance.

1.6 Surface Plasmon Band

For the absorption spectrum in UV-visible range for metal nanoparticles bigger than 5 nm, there is a strong and broad band observed, known as Surface Plasmon Band (SPB). Such types of bands are only exhibited by the nanoparticles of gold, silver and copper. Usually, all metals have predominant quantum effects rather than surface plasmon bands. The parameters that decide the shape, position and intensity of SPB are as follows:

a) Dielectric Constant of surrounding media.

b) The electronic interactions between the stabilizing ligands and nanoparticle.

1.7 Assembly

Previously, experiments were carried out to disassemble the AuNP chains; however, these experiments failed to do so. Also, it was believed that it was ethanol which caused the assembly of gold nanoparticles. But, later on, it was found that it was the residual salt in conjunction with ethanol that helped in the assembly process. Moreover, it was the dilution of salt that would disassemble the linear assembly if the AuNPs were under the protection of stronger ligand. The main job of ligand is to make sure that the nanoparticles do not aggregate into its bulk form. Thus, there was a need of a modification which would improve the short ranged repulsions. This was possible by

replacing the existing ligand with a stronger one which helped to strengthen the short range repulsions. This was necessary in order to avoid a permanent aggregation when the assemblies are formed. Thus, by virtue of the chemical addition or temperature change or any other such external stimuli, assembly and disassembly of AuNPs were manipulated in order to obtain different colour output, by utilizing the colloidal interactions. [55]

In short, there is an effect on higher architecture due to assembly of the structure at its nano scale and interaction amongst themselves. So the placement of these nanoparticles remains crucial as it controls the nature, property and behaviour at the macroscopic level. This requires to establish guidelines for process optimization and engineering methods to assemble in order to obtain a specific structure. From this, we can derive structure-property relationships so that we can predict how a particular structure would perform. This composite film helps in fabricating hierarchically ordered materials that has specific structures and performance that covers a long range of lengths and dimensions.

CHAPTER 2

BEHIND THE CURTAIN: MATERIALS AND THEIR PROPERTIES

Mechanochromic materials respond to an external pressure by changing colour. But the drawback of such materials is that they can be used only for in situ applications as they cannot retain the colour change for a longer duration of time and so it becomes difficult to measure the amount of mechanical force applied. The present study discusses a type of film which can retain the colour change for a longer duration of time even after the removal of pressure. This property of memory is possible due to the polymer's intensity and time-dependent viscous flow when an application of mechanical stress is experienced. The polymer undergoes plastic deformation because of this stress, forcing the AuNP chain to disassemble and result in a shift of plasmonic band. This depends on the applied mechanical stress.

Materials used are mainly metallic nanoparticles. In their bulk form, they have a specific natural colour and the only visible interaction with the light, that can be observed, is reflection. Nanoparticles in the form of Colloidal Solution has some ground breaking applications in recent times. Here, we review gold nanoparticles and use its solution to analyse if we could use silver nanoparticles with similar applicability and properties. Colloidal gold is one of the most important colloidal suspensions due to its excellent size, shape and optical properties. The phenomena that has been utilized is known as Localized Surface Plasmon Resonance (LSPR). We will be discussing various properties of both gold and silver nanoparticles. [56]

2.1 Colloidal Gold

Interaction of any material with light decides its optical properties. Nanoparticles offer small size, shape and colour properties. While discussing metallic nanoparticles, we take into consideration how they absorb and scatter light. Colloidal Gold is incredibly efficient in terms of absorbing and scattering light. It has wide range of colours which covers the entire spectrum and also has a colourless form. These colours depend on various factors such as size, shape, local refractive index, aggregation state and is a result of a LSPR.

Metallic nanoparticles can be produced from any metal, but the noble metals win the race, as they have the chemical inertness against most environmental conditions. The selected candidates for this task are gold and silver. This is due to the reason that LSPRs of different metals have different energies which necessarily do not fall in the visible spectrum. Nanoparticles of cadmium, indium, mercury, tin and lead are colourless. Gold nanoparticles of 20nm spheres have their LSPR peak at 520 nm which is of red colour.

2.1.1 Optical Properties

Optical properties depend on the effect of size, local refractive index and aggregation of gold nanoparticles. The larger the nanoparticle size, higher will be the wavelength of the light that it can absorb. Absorption is known by observing the peak of LSPR absorption at a particular wavelength.

In the present analysis, the composite film is fabricated by casting a nanoparticle assembly on a polymer (ligand). This plays a vital role in examining the effect of local refractive index on its optical properties. The refractive index of the solution is decided by the surroundings of the nanoparticle, which further defines the optical property of the gold nanoparticles. So, the ligands and the solvent also acts as important parameters

to influence the optical properties. The higher the refractive index, the shift of nanoparticle LSPR will be towards the longer wavelength.

The aggregation of nanoparticles is evident because we are considering assembly of NPs and so, when the overall effective formation size, shape and dielectric environment changes, there will be a change in its optical properties. It is known that the colour of the colloidal gold has a bright red colour. But it is the LSPR which decides the emission of colour and will dictate the optical properties. In short, when the LSPR frequency is in the visible region, the spectrum of gold nanoparticle will be coloured. [57].

2.1.2 Selection of the Gold Nanoparticles

The size selection of nanoparticles is crucial for this experiment because only the spheres of diameter greater than 9 nm or lesser than 100 nm will have its LSPR maxima between 517 to 575 nm which has red shades and will red-shift towards violet. For gold nanoparticles of diameter 30nm, the LSPR causes the light to be absorbed at 450nm (blue-green colour of spectrum). This light will be reflected at 700nm, which is in bright red part of the spectrum. With increase in size of the nanoparticle, LSPR will keep on shifting towards the longer wavelength and will keep on reflecting more and more red colour. Now, as the particle starts reaching the dimension of bulk materials, the wavelength will enter the infrared region and the visible wavelengths are all reflected back giving the AuNPs clear to translucent colour. To sum up, LSPR can be tuned as a function of size and shape of the AuNP, resulting in various optical applications.

Apart from size, it is the shape that determines the LSPR peak. With the change in shapes, for example, sphere, triangle, cube, prism, rod or ellipsoid, we can see the difference in the values of LSPR peaks and will lead to a variety of LSPR properties. Different shapes have different number of LSPR peaks, i.e. spherical nanoparticle has

single maxima, rod-like has 2 maxima (longitudinal and lateral). The LSPR of spherical nanoparticle is red-shifted by a large amount before entering near-infrared region.

An important aspect to note is that the localized surface plasmon resonance peaks are very sensitive to the thickness of the gold layer and so if we consider a nanoshell coating of a silica sphere and a solid gold nanosphere, the former will be red-shifted compared to the latter. As discussed earlier, the surrounding environment plays an important role in defining its optical property. It is the nature of the ligand and the nature of the bulk medium that will decide the LSPR maxima of the nanoparticle. For example, if we take into consideration a 5.2 nm Au NP and if the solvent is changed from 1.33 to 1.55 (refractive index), then there is an 8 nm red-shift in the peak. It is to be noted that scattering is the main tool which helps the chromic response. It is much more efficient than fluorescence. For a 80 nm Au NP and a blue light of 445 nm wavelength, it will scatter 106 times more than fluoresce in.

It is important to prevent unwanted aggregation of nanoparticles and for that, a layer of ligands coating is attached to their surfaces. To understand this, if we consider a 5.2 nm diameter spherical Au NP, then there are approximately 2950 atoms in the surroundings and most of them are on the nanoparticle's surface.

Modification of LSPR is also noticed by the addition of excess salt to the solution and the surface charge neutralizes on the Au NP, helping them to aggregate with much ease. This will cause the colour change from red to blue. By coating the nanoparticles with polymers or small molecules or some ligands, the aggregation minimizes by the virtue of surface chemistry. This modification has innumerable applications in chemical, biological, engineering and medical applications. Thus, different ligands will give different levels of stabilization and different chemistry and on combining this with the chromic properties of metallic nanoparticles, they give rise to wide range of optical applications and result in innovation in "smart" technologies.

2.2 Colloidal Silver

Colloidal silver is a solution of liquid in which silver nanoparticles are suspended. It has a major medical application as it is claimed to have "cure-all" properties. It has a distinct thermal, electrical and optical properties which can be used in sensor technologies. The main properties of Ag NPs are their high electrical conductivity, stability and low sintering temperature. There is an increase in the demand of antimicrobial coatings and significant research has been carried out on that front. The increase in the medical treatment is due to the fact that the medical devices containing Ag NPs release low level of silver ions that provides protection against bacteria.

In order to optimize the performance of the device, it is important to understand the change in size, shape, surface and aggregation of Ag NPs after integrating with the selected polymer. Usually characterization of Ag NPs is carried out by the transmission electron microscopy (TEM), dynamic light scattering for the particle size analysis, Zeta Potential measurements and UV-Vis spectral analysis to check consistency of materials.

2.2.1 Optical Properties

For an efficient sensor, it is important that the optical properties are properly harnessed when we make use of metallic nanoparticles. We have studied the properties of gold nanoparticles and their efficiency in absorbing and scattering of light but silver is considered to be a better option when it comes to scattering of light. Apart from its extraordinary absorbing power, the colour of the AgNP depends on the size and shape of the particle. The extinction profile (scattering + absorption) of AgNP is 10 times its physical dimension. It is because of the strong scattering pattern that it is possible to view these particles in a normal microscopic device. When 60 nm Ag NPs are viewed

under a dark field microscope, they appear as bright blue point source scatterers, which is due to the LSPR peak at 450 nm wavelength.

In case of AgNP, the unique aspect is that, by changing particle size and local refractive index, the LSPR peak can be manipulated from 400 nm to 530 nm, which is a colour change from violet light to green light. By changing the shape from sphere to rod to plates, we can shift this LSPR from visible to infrared region of the electromagnetic spectrum.

2.2.2 Surface Chemistry

In a solution, there is an association of molecules and nanoparticles which establishes a double layer of charge helping it to stabilize the particle and stops from aggregating. For instance, there is a weak association of Ag NP when suspended in a dilute aqueous citrate buffer. The selection of this buffer is due to the fact that the weakly bound capping agent provides longer stability and so can be readily displaced by other molecules such as thiols, amines, polymers and proteins.

2.3 Viscoelastic Behaviour of Polymers

The property which plays a crucial role in developing such sensors is viscoelasticity in polymers. It is a combination of viscous and elastic nature of a material, when acted upon by an external pressure resulting in deformation. As will be discussed later, the sensor is produced by casting a film on a polymer and it is this polymer which will decide the material property. Generally, viscoelastic materials exhibit time-dependent strain. [2]
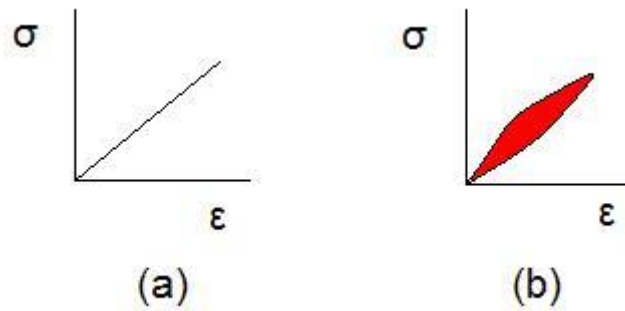
Figure 2.1 a) Stress–strain curves for a purely elastic material b) Stress-strain curve for a viscoelastic material.

Source: https://en.wikipedia.org/wiki/Viscoelasticity.

Figure 2.1 shows the difference between an elastic and a viscoelastic material. The red area is a hysteresis loop and it shows the amount of energy lost (as heat) in a loading and unloading cycle. It is equal to $\oint \sigma \, d\varepsilon$ where σ is stress and ε is strain. In an elastic material, there is no loss of heat (energy) when the stress is applied and removed. In the case of a viscoelastic material, there is a heat loss during the deformation and the nature can be shown by looking at the hysteresis loop in Figure 2.1(b). When stress is applied on the polymer, the area under the pressure undergoes a molecular rearrangement and that part of the long polymer chain changes its orientation and it is known as creep. This rearrangement will keep the solid formation intact even during application of stress and will create a back stress, which on removal of the original stress will help in getting the polymer back to its original form.

Viscoelastic materials can exhibit responses as featured by a solid and liquid. This is the reason why the mechanical properties of such materials depend on time, as it is the intrinsic nature of the material. The special characteristic of viscoelastic materials is that it has a memory of past forces experienced by the material, which retains for a longer period of time that eventually fades away. Thus, if pressure is applied on such materials, the amount of pressure will be stored by them.

2.3.1 Newton's Law of Viscosity

The materials which follow Newtonian fluid have a linear relationship between shear stress and shear strain. Only such materials will obey Newton's law of viscosity. Every other material will be considered non-Newton fluids. Figure 2.2 shows the difference between the graphs of both these fluids.
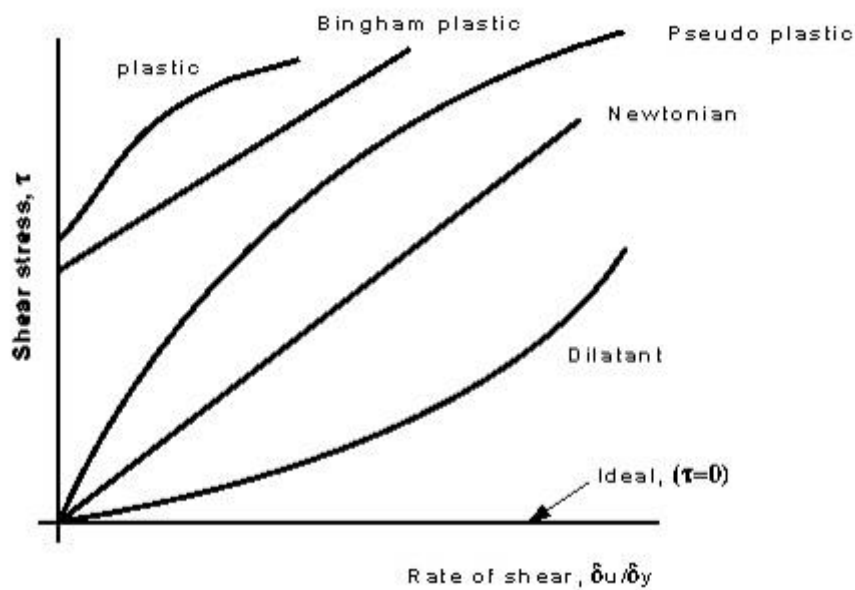
Figure 2.2 A plot of Shear stress τ vs Rate of Shear, showing the difference between the Newtonian and non-Newtonian fluid.

Source: http://www.efm.leeds.ac.uk/CIVE/CIVE1400/PDF/Notes/section1.pdf.
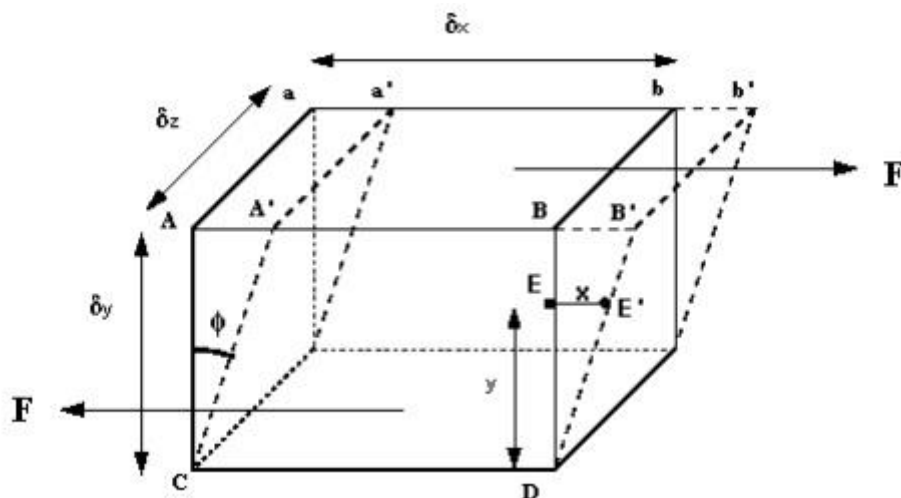
Figure 2.3 A fluid element when shear stress is applied.

Source: http://www.efm.leeds.ac.uk/CIVE/CIVE1400/PDF/Notes/section1.pdf.

The law that governs this thesis is Newton's law of viscosity and it is derived as follows:

We will begin with calculating shear stress by supposing that the area on the top in Figure 2.3 is under the influence of the shear stress, which is force per unit area

$$A = \delta s \times \delta x \tag{2.1}$$

$$\text{Shear stress, } \tau = \frac{F}{A} \tag{2.2}$$

angle $\emptyset$ defines shear strain, which is the deformation due to shear stress:

$$\text{Shear strain } \emptyset = \frac{x}{y} \tag{2.3}$$

If the particle at point E (Figure 2.3) moves under the shear stress to point E' and it takes time t to get there, it has moved the distance x. For small deformations, we can write the following:

$$\text{Rate of shear strain} = \frac{\emptyset}{t} \tag{2.4}$$

$$= \frac{x}{ty} = \frac{x}{t}\frac{1}{y} \tag{2.5}$$

$$= \frac{u}{y} \tag{2.6}$$

where $\frac{x}{t} = u$ is the velocity of the particle at E

Now, shear stress is proportional to the rate of shear strain, we get

$$\tau = \text{Constant x } \frac{u}{y} \tag{2.7}$$

$\frac{u}{y}$ is the change in velocity with velocity gradient y and may be written in the differential form $\frac{du}{dy}$

The constant of proportionality is known as the dynamic viscosity, μ of the fluid and gives us the equation known as Newton's law of viscosity; that is:

$$\tau = \mu \frac{du}{dy} \tag{2.8}$$

Thus, in Hook's law, stress is linearly related to strain, whereas in Newton's law for viscosity, stress is linearly related to the rate of change of strain or strain rate. [3]

2.3.2 Kelvin-Voigt Model
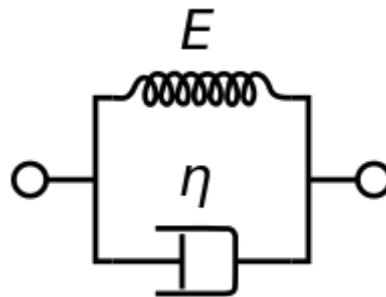
Figure 2.4 A schematic of Kelvin-Voigt model.

Source: https://en.wikipedia.org/wiki/Kelvin%E2%80%93Voigt_material

Due to the viscoelastic behaviour of the material, we will mainly observe two types of phenomena: creep and stress relaxation. This work makes use of the mechanical model known as Kelvin-Voigt model to understand the creep behaviour of the polymers. [4]

This model is constructed using elastic springs and viscous dashpots. This elastic spring (Hookean) and Newtonian elastic spring are connected in parallel as shown in Figure 2.4.

According to Hooke's law in elastic spring: $\sigma = E\varepsilon$ $\qquad$ (2.9)

Viscous dashpot follows Newton's law of viscosity: $\sigma = \eta \frac{\partial \varepsilon}{\partial t}$ $\qquad$ (2.10)

Here, the spring has the modulus E and a dashpot of viscosity η. Stress σ is applied constantly at $t = 0$. Dashpot is a damper, acting by the virtue of viscous friction, to resist the displacement motion. The direction is opposite to the velocity, so that it resists the motion and absorbs the energy. Thus, due to dashpot, instantaneous extension is denied. Deformation occurs at a varying rate and after a time, depending on viscosity, spring reaches maximum extension.
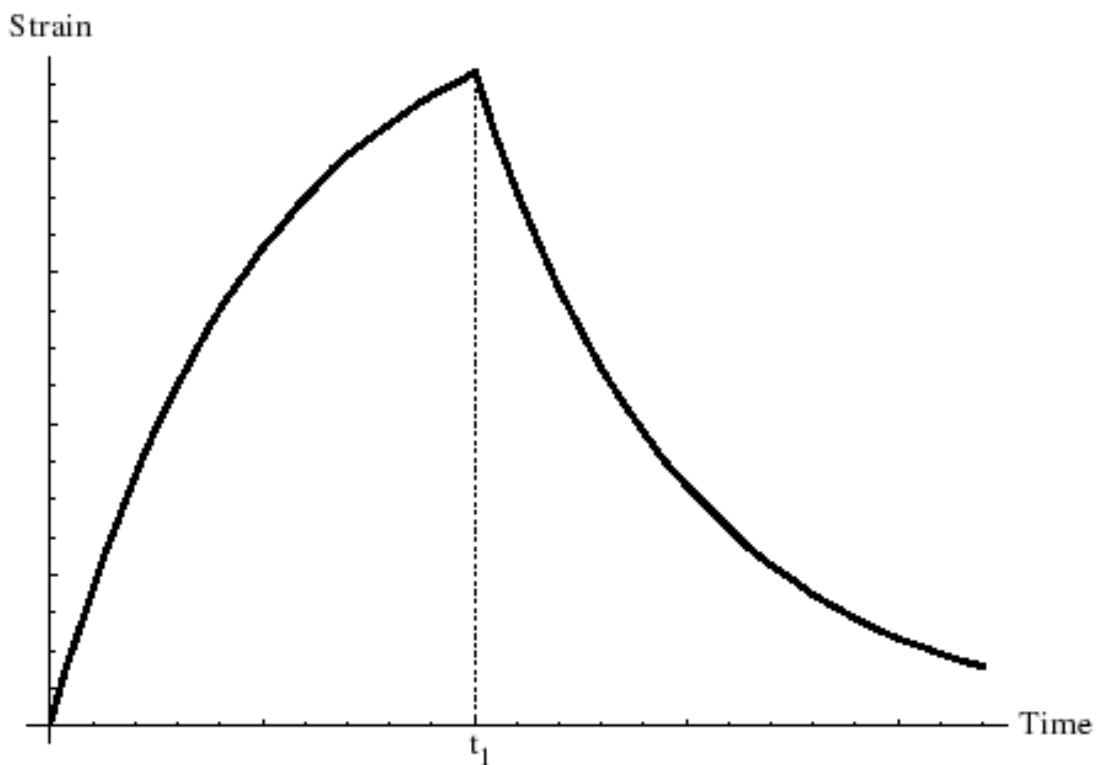
Figure 2.5 Plot of strain vs time and the decreasing curve after t_1 is the recovery time.

Source:
https://en.wikipedia.org/wiki/Kelvin%E2%80%93Voigt_material#/media/File:Kelvin_deformation_2.png.

As can be observed in Figure 2.5, the recovery occurs after the stress is removed. Thus, the stress for both the components will be as follows:

$$\text{For spring } \sigma_1 = E\varepsilon_1 \qquad\qquad (2.11)$$

$$\text{For dashpot } \sigma_2 = \eta\, \frac{\partial \varepsilon_2}{\partial t} \qquad\qquad (2.12)$$

Total stress and total strain are given by the summation of individual stress and strain.

$$\sigma_{total} = \sigma_{1} + \sigma_{2} \tag{2.13}$$

$$\varepsilon_{total} = \varepsilon_{1} + \varepsilon_{2} \tag{2.14}$$

Thus, we end up getting total stress as,

$$\sigma_{total} = E\,\varepsilon_{1} + \eta\,\frac{\partial\varepsilon_{2}}{\partial t} \tag{2.15}$$

Now, on solving for $0 < t < t1$, when the stress is,

$$\sigma_{total} = \frac{E}{\eta}\int_{0}^{t} dt = \int_{0}^{\varepsilon}\frac{d\varepsilon}{\sigma/_{E}-1} \tag{2.16}$$

where $\frac{\eta}{E}$ has the dimensions of time and represents the rate of deformation and is also known as retardation time ŕ. Thus, by integration, we get:

$$\frac{t}{\acute{r}} = \ln\left(\frac{\sigma/_{E}}{\sigma/_{E}-\varepsilon}\right) \tag{2.17}$$

and finally, the strain will be:

$$\varepsilon = \frac{\sigma}{E}\left[1 - \exp\left(-\frac{t}{\acute{r}}\right)\right] \tag{2.18}$$

where, ŕ is the retardation time.

The major limitation of this model is that it will not help in measuring the stress relaxation because at constant strain, a dashpot cannot relax. Thus, the 2nd term in the total stress formula will be 0 and thus the total stress will be only the value of stress due

to elastic spring. Thus, by the virtue of Kelvin- Voigt model and Newton's law of viscosity, we get the relation between stress and irreversible deformation as:

$$\varepsilon(to) = \int_0^{t0} \frac{\sigma(t)}{\eta} \, dt \qquad (2.19)$$

CHAPTER 3

EXPERIMENTAL APPROACH

3.1 Fabrication of AuNP composite films
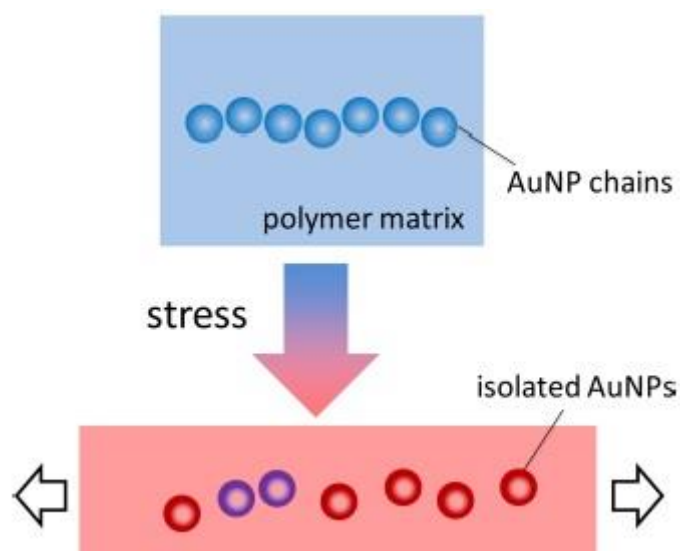
Figure 3.1 Schematic of the formation of colorimetric stress responsive film by disassembly of gold nanoparticles.
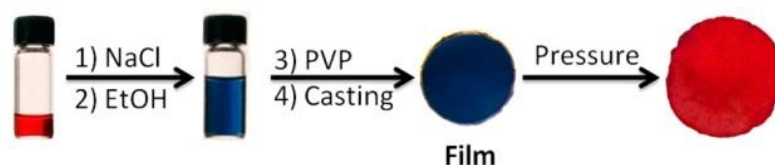
Figure 3.2 Illustration of film fabrication procedure and compression test results.

Fabrication of this film is a very crucial task as it will decide the parameters of pressure and time. It will also decide the applicability of the sensor. Figure 3.1 shows the schematic of the working principle of the sensor. Figure 3.2 describes an overview of how the AuNP forms a composite film with the polymers. AuNPs of the size 15nm were synthesized by Turkevich method explained below.

3.1.1 Turkevich method – Sodium Citrate Sols

This is a method of the synthesis of colloidal gold and is prepared by sodium citrate sols. This preparation is termed as the standard sodium citrate sol. It begins by heating a 95 ml. of chlorauric acid solution, which contains 5 mg Au, till it starts boiling. At this point, 5 ml of 1% sodium citrate solution is added and is mechanically stirred. By the end of 5 min, a dark coloured solution was prepared, which could be either greyish-pink or greyish-blue, which eventually turned out to be deep wine red. Figure 3.3 shows the gold nanoparticles which are prepared by this method. The main feature about this preparation is that it is reproducible and the diameter spans around 200 ± 15 Å. Also, the root-mean-square deviation is of 12.5%. [9]
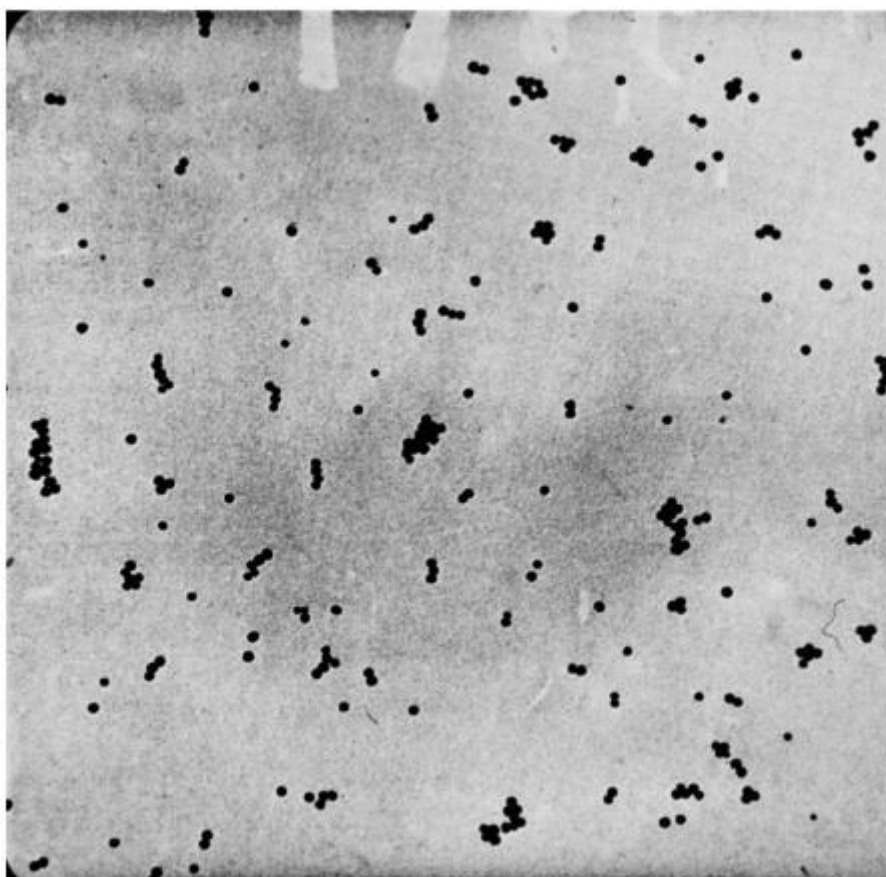
Figure 3.3 Electron Micrograph of gold sol reduced with sodium citrate with a magnification of 50000 diameters.

Source: A Study of the Nucleation and Growth Processes in the Synthesis of Colloidal Gold by John Turkevich, Peter Cooper Stevenson and James Hillie.
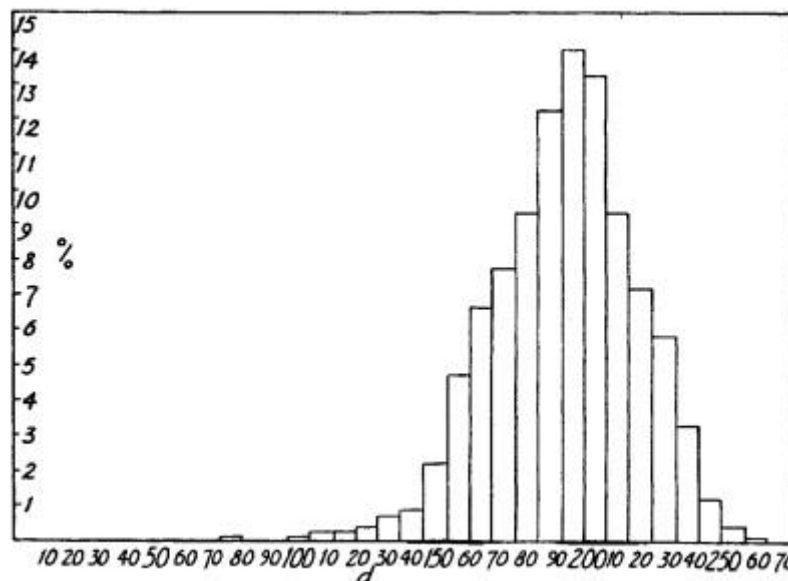
Figure 3.4 A plot of size distribution of a standard citrate sol.

Source: A Study of the Nucleation and Growth Processes in the Synthesis of Colloidal Gold by John Turkevich, Peter Cooper Stevenson and James Hillie.

Figure 3.4 shows the distribution of the size of nearly 1046 particles prepared by this method. It has to be noticed that the distribution is not symmetrical, rather there is a peak around 200 Å.

There are different effects on the size of these particles under various temperature, concentration of reagents and the dilution of the solution. When the temperature is decreased by 10 ° C, the time taken for the reaction to get completed increases by the factor of 2. The completion of reaction is being judged by the deepening of the colour. Also with that, the mean particle size and the root mean square deviation decreases. The effect of temperature is given in Table 3.1. [5] - [9]

Table 3.1 The Effect of Temperature on the Sodium Citrate Sol [9]

Temp ° C	Approx. time to complete the reaction (min)	Mean Particle Size (Å)	% Deviation
100 (Standard)	5	200	12.5
80	25	165	8.1
70	45	180	8.6

3.1.2 Synthesis of citrate-capped AuNP
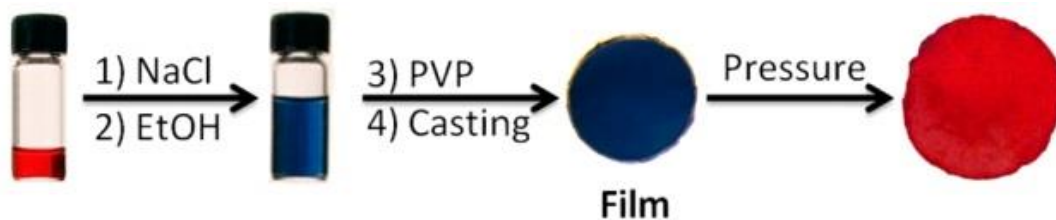
Figure 3.5 Outline of process of fabricating AuNP chain-polymer composite film.

Source: Colorimetric Stress Memory Sensor Based on Disassembly of Gold Nanoparticle Chains by Xiaogang Han, Yiding Liu and Yadong Yin.

The overview of the fabrication process of Au NP composite film is shown in Figure 3.5. In this analysis, a slightly modified method of Turkevich is applied and for that, gold nanoparticles of 15 nm were used. Now, a ligand exchange process has to be performed. As the name suggests, it is a reaction in which one ligand in a complex ion is replaced by another one, which can be either the stronger one or more suitable for the requirement. Here, bis(p-sulfonatophenyl)-phenylphosphine (BSPP), a stronger ligand compared to citrate, is introduced to the surface of the Au NPs. [10][11]

The process of assembly starts from hereon. In the solution of ethanol, an iota of NaCl is added to increase the ionic strength of the solution. Because of this addition, it becomes easier to assemble the AuNPs into linear chains and due to this, the colour changes from ruby red to blue. The increase in ionic strength helps in linear assembly because it screens the electrostatic repulsion between particles and helps triggering it.

The next step is to produce a composite film. For that, Polyvinylpyrrolidone (PVP, MW = 360 000) was dissolved in the solution to form a viscous suspension. Removing solvent becomes important as the suspension has to be casted onto a glass to produce a composite film. The solvent is removed slowly by evaporation. The chemical synthesis of metal nanoparticles with well-controlled shapes, sizes, and structures is a practical reality. The major requirement seems to be the selection of a capping reagent

that is able to chemically modify various faces of a metal with an appropriate selectivity.

Polyvinylpyrrolidone (PVP) has high solubility in water and ethanol and that is the reason it has been selected as polymer matrix. Its optical absorption in the visible region is very low and it forms very good films. The use of coating nanoparticle with surfactant or polymer is to prevent agglomeration of the particles due to high surface energy of nanoparticles. It also controls the size of the particles during synthesis process. PVP acts as an additional capping agent and ascertains their homogeneous dispersion in the polymer without disturbing the chain structure of the matrix. [11]-[19]

After the assembly, we need to make sure that we can disassemble when necessary. This is being taken care of by the adhesion arising from the bonding between pyrrolidone groups and the gold surface. We notice that the colour of the Au NP chain is blue and that colour remains the same even after forming the Au NP-PVP composite film.
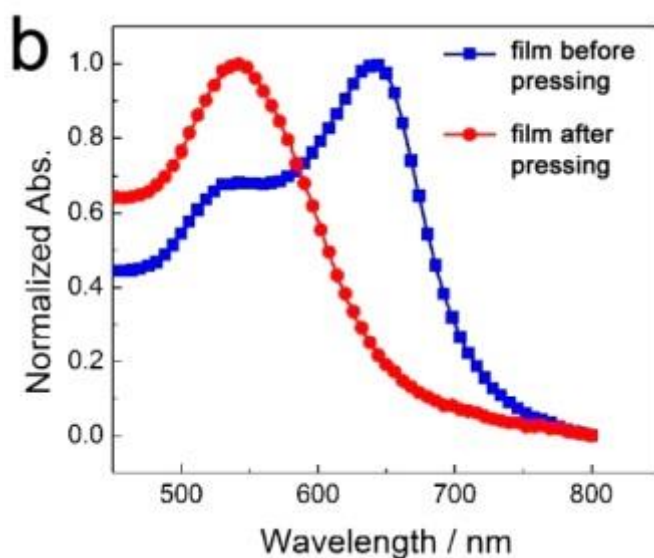
Figure 3.6 UV-vis extinction profiles before and after pressing.

Figure 3.6 shows that the composite film maintains its chain structure even after pressing. Before pressing, the coupling peak is in the visible range at 650 nm. The

composite films were checked after 30 days of storing it at 4 °C at 50% humidity and was observed that the extinction profile remained unchanged. [1]

3.2 Fabrication of Ag NP Composite Films

The procedure for the synthesis of uniform silver nanoparticles is by making use of sodium acrylate (SA) as reducing and stabilizing agent. In this synthesis of silver nanoparticles, Poly- (sodium acrylate) (PSA) has been used as a stabilizing agent prepared from silver salts using gamma radiation or chemical reduction. There is one more process discussed which prepares Ag NP using PVP and this will help in comparing the process with that of Au NP which is also fabricated using PVP.

3.2.1 Preparation of Silver Nanoparticles using Sodium Acrylate

An aqueous solution of $AgNO_3$ (50 mL, 3 mM) was refluxed for 5-10 min under an argon atmosphere, and a warm (50-60 °C) aqueous solution of SA (25 mL, 160 mM) was added quickly. Reflux was continued until a yellowish-brown solution was obtained (approximately 30 min). This solution was filtered through 0.45 µm Millipore syringe filters to remove any precipitants, and the filtrate was stored at room temperature in the dark under an argon atmosphere.

Getting a narrow size distribution is the primary target in the preparation of the nanoparticle. In the case of Ag NP, it is a bit difficult to obtain the narrow size distribution as the colloidal silver is highly sensitive to oxygen. A starlike or leaflike structure is formed while preparing silver nanoparticles by the reduction of silver salts using gamma radiation in the presence of citrate. [20]

The experiment was able to overcome the stability issue of silver nanoparticles when prepared using sodium acrylate under anaerobic conditions and the synthesis of

stable Ag NP with characteristic plasmon resonance band at 432 nm and its TEM

images are shown in Figure 3.7. Mostly, the particles are in the range of 18-40 nm.
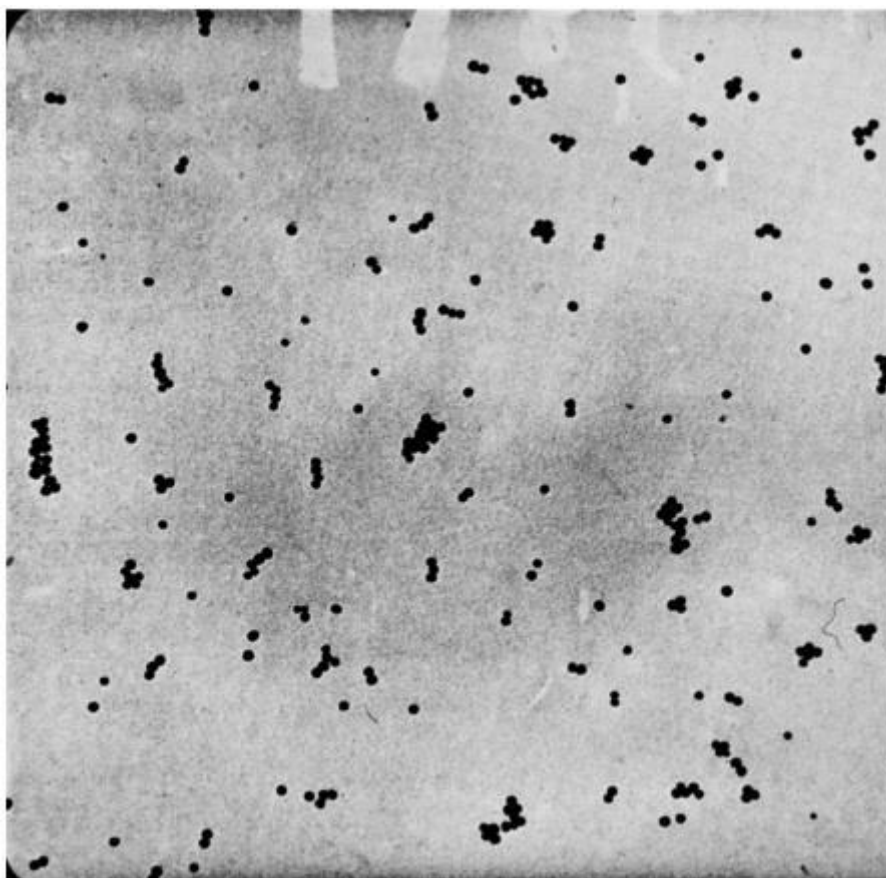
Figure 3.7 TEM micrograph of silver nanoparticles using sodium acrylate.

Source: Preparation of Acrylate-Stabilized Gold and Silver Hydrosols and Gold-Polymer Composite Films by Irshad Hussain, Mathias Brust, Adam J. Papworth and Andrew I. Cooper.

3.2.2 Preparation of AgNP using PVP

There are some fundamental differences of the effect of PVP on gold and silver. Thus,

there are different implications on the structures of the Au NP-PVP and Ag NP-PVP

composite films. When the Au NP is formed via reduction of $HAuCl_4$, the concentration

of PVP changes the UV-vis absorption, λ_{max}, size and shape of the resultant AuNPs. On

the contrary, when $AgNO_3$ is reduced to prepare Ag NPs, the concentration of PVP

changes only silver nanoparticle's population density. The seeds of the crystal

structures control the shape specification of Ag nanoparticles, for example, cube, sphere, bipyramid, wire, etc. [21]

A mixture of N-methyl-2-pyrrolidinone, PVP and AgNO₃ is heated at 200 ᵒ C for 120 minutes and by the end of the two hours, a colour change of the solution from colourless to dark brown was observed. Ag particles of 2 nm were observed in a TEM micrograph. They will serve as the seeds for further growth into larger Ag NPs. These seeds will only grow to form Ag nanospheres and so with the fabrication of Ag NP-PVP, no other shape is possible.
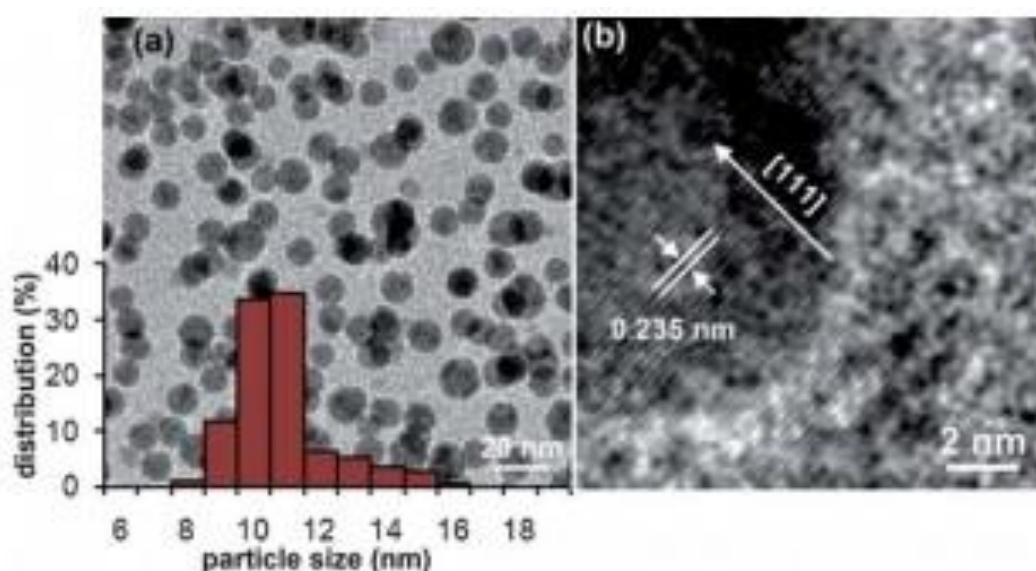
Figure 3.8 a) TEM image and size distribution of Ag NP from the nanocomposite films. b) A HR-TEM image of typical Ag NP.

3.2.3 Summary

Polymeric thin film composites consisting of nearly monodispersed silver and gold nanoparticles were fabricated via a one-step polymer-assisted technique, with PVP as the capping and reducing agents. This environmental friendly synthetic method is very simple; it involves minimum amount of organic solvent and requires a very short reaction time of less than 1 min. The morphological control of Au nanoparticles, from

tetrahedral to nanocubes to dodecahedral, is achieved by varying the concentration and molar ratio between the metal precursor and polymer. Following the same procedure for the synthesis of Ag nanoparticles, we find perfectly single crystalline, spherical Ag NPs with a very narrow size distribution. These composite thin films, with homogeneously dispersed nanoparticles, exhibit optical properties that are closely associated with that of the pure nanoparticles and they could have commercial implications in nonlinear optics and antimicrobial surfaces. [22]

3.3 Characterization of Au NP

Optical absorption profiles of the films were measured using a Varian Cary 50 UV-Vis spectrophotometer. The area change of the sample was determined by taking digital images of the sample before and after the compression test, with a ruler to reference the scale followed by measuring the size of the sample from the images. The thickness of the sample was measured using a micrometer. TEM measurements were performed on a Tecnai T12 with an accelerating voltage of 120 kV.
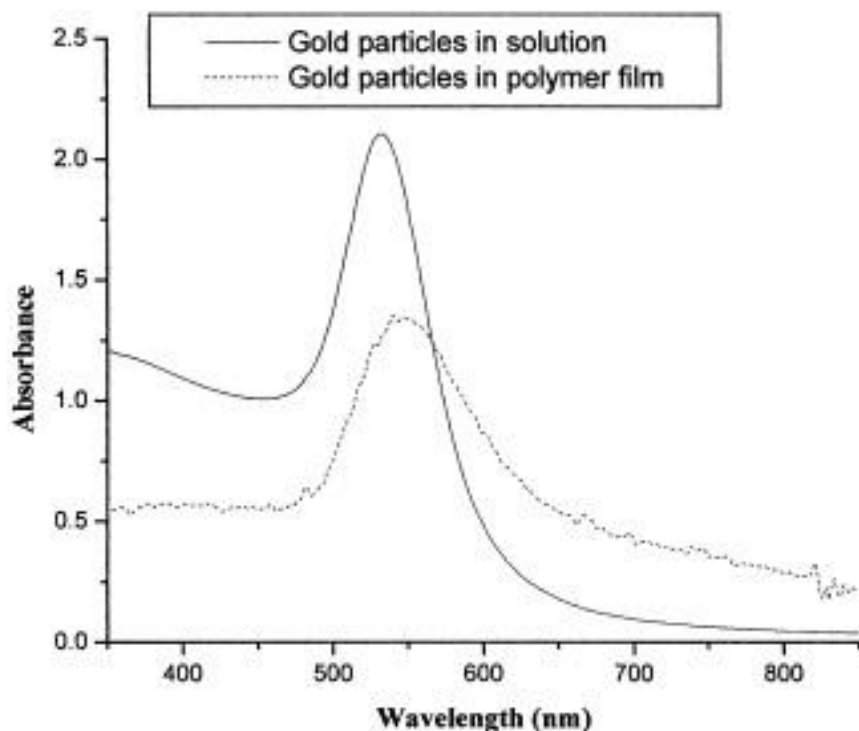
Figure 3.9 UV-visible spectra of polymer-stabilized gold nanoparticles before and after thin film formation.

Source: Preparation of Acrylate-Stabilized Gold and Silver Hydrosols and Gold-Polymer Composite by Films Irshad Hussain, Mathias Brust, Adam J. Papworth and Andrew I. Cooper.

3.4 Characterization of AgNP

Transmission Electron Microscopy (TEM), Scanning Electron Microscopy (SEM) and Atomic Force Microscopy (AFM) are the analytical techniques used to measure shape and size of metal nanoparticles. Dynamic Light Scattering (DLS) or analytical disc centrifugation are the techniques used to measure the aggregate state by measuring the effective size of the particles in the solution. The spectral properties of the silver nanoparticles in the solution can be analysed if we want to know more about the silver nanoparticles as they exhibit unique optical properties.
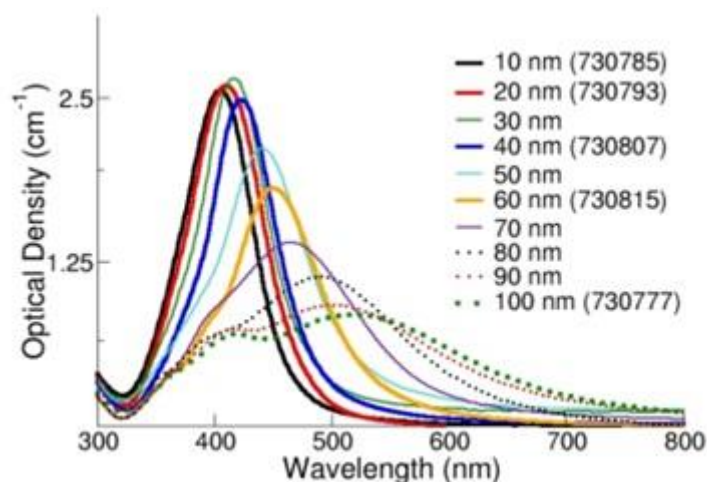
Figure 3.10 Extinction (scattering + absorption) spectra of silver nanoparticles with diameters ranging from 10-100 nm at mass concentrations of 0.02 mg/mL.

Source: http://www.sigmaaldrich.com/materials-science/nanomaterials/silver-nanoparticles.html.

The plasmon resonance peak depends on the diameter of the silver nanoparticles and the spectral response of different diameter is shown in Figure 3.10. With the increase in diameter, there is a red shift of the peak of plasmon resonance and it broadens. As longer wavelengths, there comes a point after which if the wavelength increases, there comes a 2nd peak which is due to the quadrupole resonance which has different electron oscillation pattern than primary dipole resonance. Every plasmonic nanoparticle with a specific size and shape has a unique peak wavelength, peak width and effect of secondary resonances which acts like their fingerprint. Also, nanoparticles change over time and they can be monitored using UV-vis spectroscopy. Individual nanoparticle acts differently than the way they act while aggregated. This is because the aggregation causes the NPs to electronically couple with each other and it has different surface plasmon resonance than the individual particle. The coupled nanoparticles will be red shifted than the individual particles and the intensity will be seen increasing towards the red/infrared region of the spectrum.

Figure 3.11 shows this effect. With the addition of saline, the optical response of AgNP destabilizes. Carefully monitoring the UV-Visible spectrum of the silver

nanoparticles with time is a sensitive technique used in determining if any nanoparticle

aggregation has occurred.
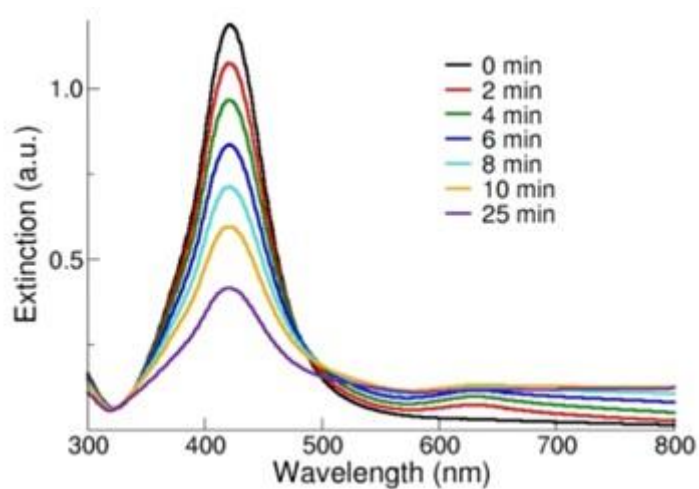
Figure 3.11 Extinction spectra of silver nanoparticles after the addition of a destabilizing salt solution.

Source: http://www.sigmaaldrich.com/materials-science/nanomaterials/silver-nanoparticles.html.

CHAPTER 4

OPTICAL PROPERTIES

The selection of the candidate and its applicability mainly depends on the spectral analysis of the particle. We analysed the preparation procedure of the Au NP and Ag NP, the fabrication of the composite film, the size and shape.

Au NPs have been intensively studied as the technological advancement is more on this front. The unique part of this study is to understand and apply the knowledge from the extinction profiles of Ag NPs to see whether it can substitute the already existing Au NPs.

The noble metal nanoparticles exhibit this unique optical property in which when the incident light has a frequency similar to the excitation of the collection of electrons in the conduction band, a band is observed in UV-visible range usually and this band is named excitation band. After going through various procedures and experimentation, the extinction profiles are usually affected and this will help us in knowing whether the respective candidates (Au NP and Ag NP) are useful for any specific application. [23]

4.1 Optical and Spectral Analysis of Au NP Films

In order to study the spectral characteristics of Au NP, firstly they are subjected to a compression test which will change their dimensions and shape of the film. This will redefine their extinction profiles and this will decide their characteristics.

4.1.1 Compression Test of Au NPs

The films prepared had an area of 3 mm^2 with the thickness of 0.25 mm and they were cut into circular pieces by a homemade puncher. Now, to initiate the compression test, the circular films were first introduced in the compressor and forces were applied for a constant period of time with a force gauge. The force is calculated by the initial pressure in a given area. Also, it was necessary to study if the shape change affects the extinction profile of the film. For this, the morphology and extinction profile of the film, before and after pressing the film, was studied. Figure 4.1 shows the comparison of the profiles. The measurements were taken by dissolving the films in water and then taking optical measurements and performing TEM.

The extinction profiles of the film, before and after pressing, show an absorption peak at 520 nm and the morphologies showed no difference in the TEM images. This is also supported by a strong similarity of the profiles of isolated Au NPs, both before and after pressing.
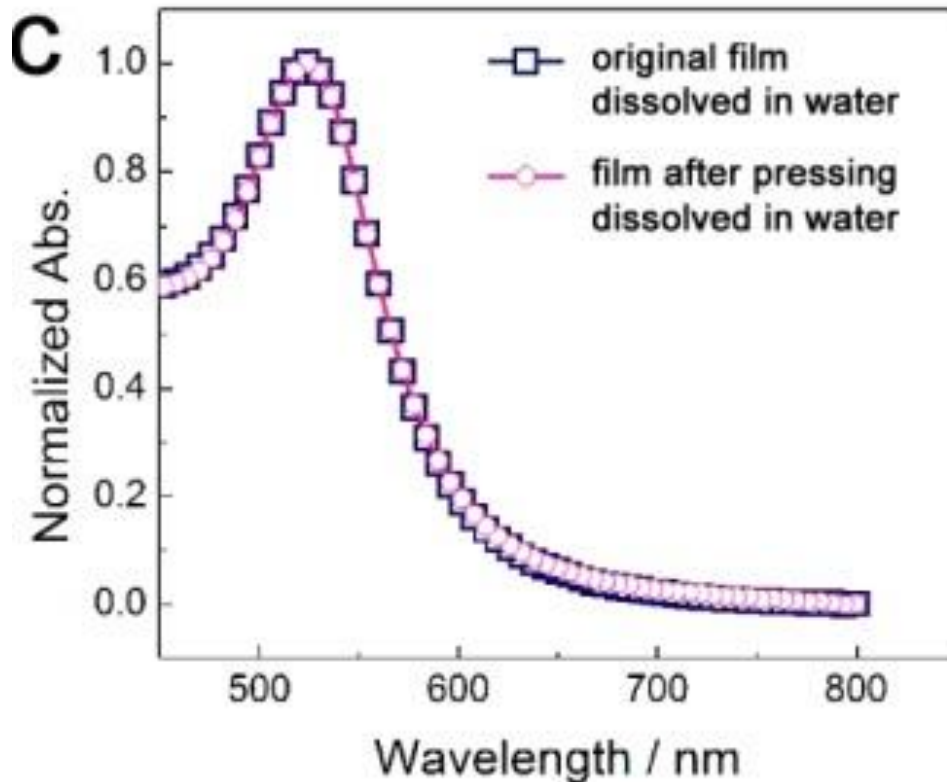
Figure 4.1 Extinction profile before and after pressing the film.

Source: Colorimetric Stress Memory Sensor Based on Disassembly of Gold Nanoparticle Chains by Xiaogang Han, Yiding Liu and Yadong Yin

A colour change from blue to ruby red was observed after an application of 1.6 x 10^5 psi to the film for 1 min. In the previous chapter, we observed (Figure 3.6) the extinction spectrum of the film after the pressure is applied and it was observed that the absorption peak was at 530 nm with a small shoulder, which corresponds to the transverse mode of the plasmon resonance. These experiments support the initial claims that the plasmon band shift is solely due to disassembly of Au NP chains during the film deformation. [1]

If the intensity of pressure and the duration of the applied stress are increased, then there is an increase in probability that the viscous deformation is irreversible. This is by the virtue of Equation 1.1. To make sure that these two parameters create considerable difference, it is necessary that there is a proper adhesion between PVP and Au NPs and only then the disassembly will have a proper effect. This was tested by applying various pressures on the film for 1 min and the results showed a consistent

blue shift of the plasmon peak with increase in the applied pressure. Also, there is a dampening of the peak with increase in applied pressure. Figure 4.2 shows the results of the investigation. If the pressure is kept increasing, then there will be a point when the spectrum of the film overlaps with the spectrum of the isolated Au NPs and makes it indistinguishable. This happens to be around 530 nm. [1]
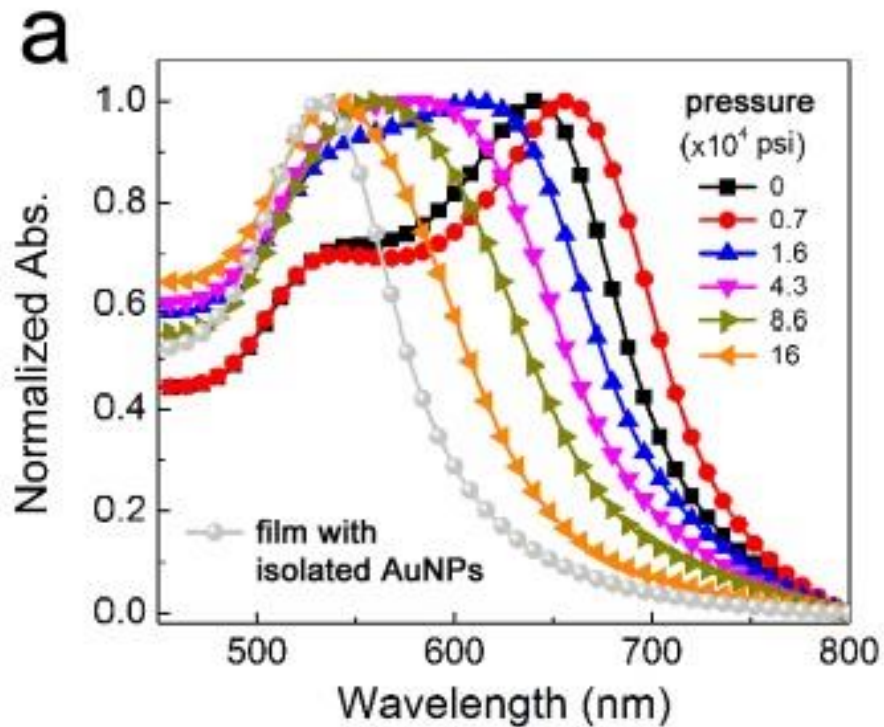
Figure 4.2 The UV−vis extinction spectra of a typical composite film after experiencing different pressures for a fixed application time (1 min).

Source: Colorimetric Stress Memory Sensor Based on Disassembly of Gold Nanoparticle Chains by Xiaogang Han, Yiding Liu and Yadong Yin

To confirm the change in plasmon band positions, continuous wavelet transform (CWT) was used to analyse the spectra for the overlapping signals and this spectra of optical change can be seen in Figure 4.3. [24]
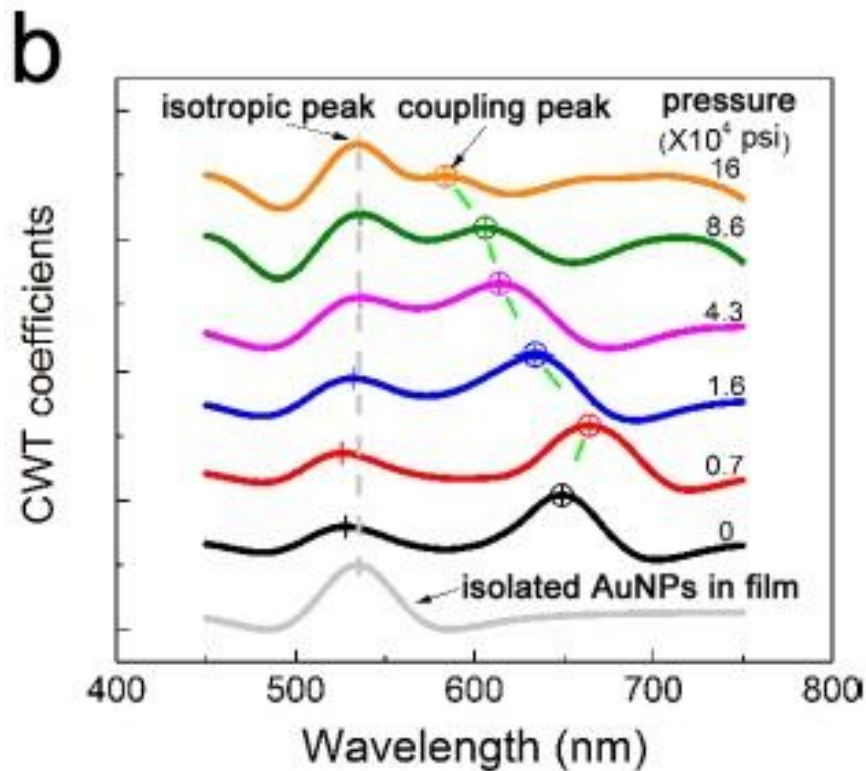
Figure 4.3 The CWT of the spectra.

With increase in pressure, there will be an increase in the area and decrease in the thickness and ultimately this results in a change in density. This was calculated at some approximation as an expansion in area by 61% than the initial area and decrease in thickness by 42%, with an enhanced density of nearly 8%. But the density did not change on increase of pressure; so it was just restricted to initial small pressure. Now, it has been stated initially that the deformation has to be inelastic in order to memorize the stress. Before reaching that point of inelastic deformation, it passes through an elastic deformation and this is the reason for initial density expansion at mild pressure. This transformation is shown in Figure 4.4. [1]
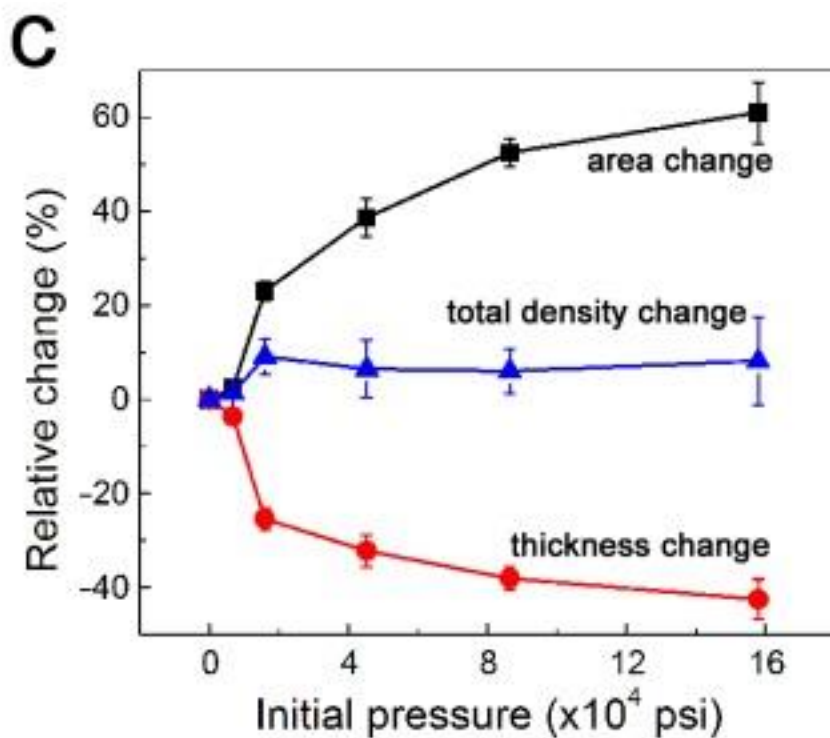
Figure 4.4 Physical deformation profiles of the films after being subjected to various pressures for 1 min.
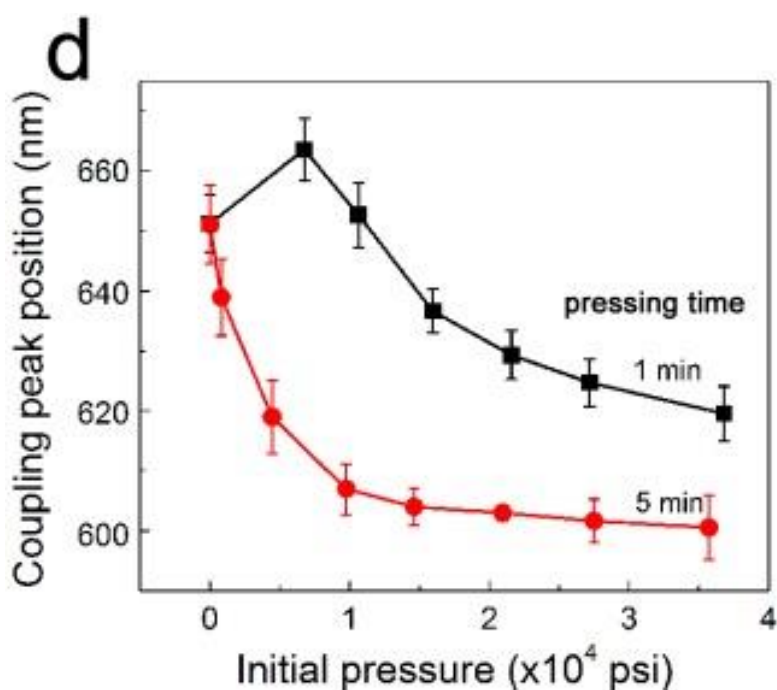
Figure 4.5 Plot of coupling peak position shift for films experiencing different pressures and application times (1 and 5 min).

Figure 4.5 shows that the coupling peak position and the amount of blue shifts remain consistent with a fixed amount of time. It can be seen that, with greater amount of deformation, there will be greater extent of blue shift and dampening. Basically, with an increased amount of stress, the amount of deformation increases and the inter particle distance keeps on increasing. Because of that, the plasmon band shifts more due to an increased amount of displacement of Au NPs. [1]

4.1.2 Effect of Elastic Deformation

The effect of elastic deformation has other implications at the early stages of compression. A mild pressure of 7×10^3 psi for 1 min will force the coupling peak to be red shifted rather than blue shift and the peak changes from 649 to 664 nm due to elastic deformation. The vertical compression at the initial stage would increase the thickness by 3.7% instead of decreasing and the lateral expansion is less, with 2.4% change in area. The reason for red shift is that initially, the compression decreases the inter-particle distance, with an increase in the order of Au NP chain and the coupling effect strengthens. Because of this, the peak shifts to longer wavelength. [1]

Basically, when the film is under stress, the Au NPs undergo a combination of elastic and inelastic deformation and thus might move closer to each other. This will result in an increase in the coupling interaction. Inelastic deformation has a major effect at higher pressure, resulting in blue shifting the plasmon peak due to the lateral polymer flow causing the separation of AuNPs in the chain. A red-shift can be noticed approximately around 530 nm due to increased isolated Au NPs at higher pressures. Figure 4.5 shows an important result, where the applied pressure is kept constant but the duration of stress is increased from 1 to 5 min, resulting in a significant blue shift of the peak. This is not only restricted to just high pressure, but even a mild stress for a longer duration can result in a considerable colour change with large band shifts.

4.2 Disassembly of Au NPs

After reporting the complete process from the nature of gold NPs to the process of their production to their assembly to their casting to a polymer to the extinction profiles, we analyse the main aspect of this thesis. It is the disassembly of the AuNPs that causes the extinction profile to shift and results in the colour change of the film. So understanding disassembly and how it causes the colour change plays a major role. The unique property of this film, compared to other mechanochromic materials, is that the film memorizes the stress. This is caused by the inelastic deformation of the polymer, that causes the assembly to spread out and so it becomes necessary to understand the consequences of disassembly.

To begin with, there should be a pre-defined value of the duration of stress application and the strength of applied pressure for a particular type of composite film. This will give a range in which the film is useful for a corresponding application. The usage of such films are usually in the day to day commodities and they would usually fall under room temperature or lower temperature. PVP loosens up only if the temperature is considerably high and so it is usually very hard at room temperature. This makes it difficult to deform under mild pressure. Thus, only a considerably high pressure would cause an inelastic deformation and so it is a major hurdle to widen the pressure range. To achieve this, we can either lower the hardness or decrease the viscosity by doping PVP with plasticizers that will increase the fluidity.

It is a known fact that the proton donors, i.e. –OH groups donate H to the acceptors to form carbonyl group by forming H-bonds. It is because of this reason that PVPs are miscible with the hydroxyl group which are contained in small molecules. These molecules, when added in PVP, help in decreasing the viscosity and make it more fluidic. There are various molecules which fit this purpose but after analysing couple of research papers, the best suited option is poly(ethylene glycol). [1] [26]

4.2.1 Effects of PEG

The plasticizer, well suited for this application, is PEG-400. Figure 4.6 shows the chemical structure of PEG. It has a hydrophilic property and is soluble in water, acetone, glycerine, glycol and in few aliphatic hydrocarbons. Care is to be taken when molecules are added in the polymer as they are more likely to disturb the assembly of nanoparticles. But, the addition of PEG does not interfere with the structure of Au NPs and it gels in with PVP easily. PEG 400 is in fact miscible with other polymers and is widely used. Figure 4.7 shows the miscibility of PEG 400 with other polymers and with PVP. It shows that the miscibility of PVP is the least, in a way that it is miscible enough to not destroy the polymer and there remains some solidity in order to sustain its form.
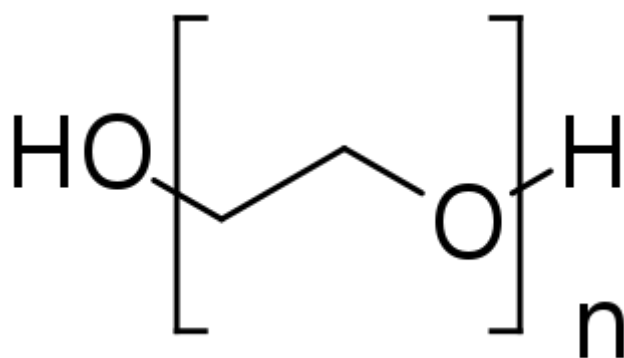
Figure 4.6 Chemical Structure of PEG

Source: Wikipedia
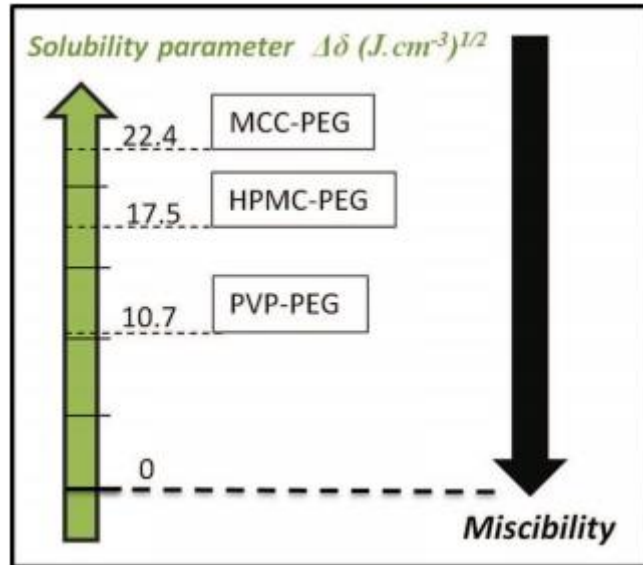
Figure 4.7 Miscibility of PEG with MCC, HPMC and PVP

The fluidity of PVP is directly proportional to the amount of PEG added. So more the content of PEG-400, higher will be its fluidity. With the increase in fluidity, the composite film will be more responsive to the external pressure. This will result in the change in the optical property of the composite polymer film. [27]

We have already analysed the effect of the application of pressure of 1.6×10^4 psi for a duration of 1 min on the composite film. Now, after doping the film, the physical deformation and colour changes are studied and is shown in Figure 4.8.
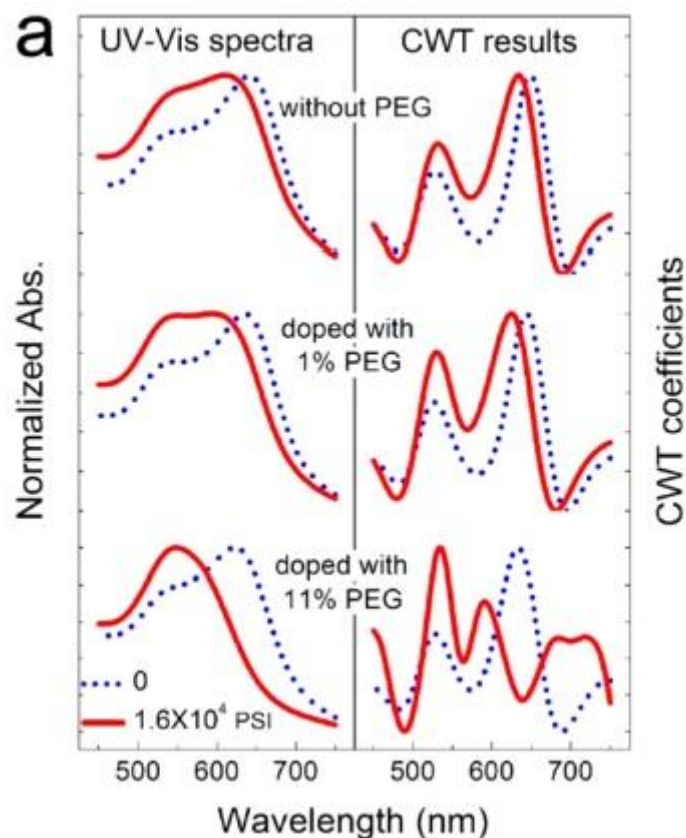
Figure 4.8 UV-vis extinction spectra (left) and their CWT profiles (right) for films doped with different amounts of PEG before (dot) and after (line) being treated with 1.6×104 psi of pressure for 1 min

Source: Colorimetric Stress Memory Sensor Based on Disassembly of Gold Nanoparticle Chains by Xiaogang Han, Yiding Liu and Yadong Yin

The plot of the effect on extinction profiles by the addition of PEG shows that the blue shift of coupling peak without doping is from 649 to 635 nm. When doped with just 1% PEG, the blue shift is from 646 to 627 nm. This shift increases when doped in more quantity, i.e., when doped with 11% PEG; the shift is from 636 to 591 nm. Thus, on an increased amount of PEG doping, the disassembly is even more pronounced.

With different amounts of doping, the optical properties of the composite film highly depend on the applied pressure. This result can be seen in Figures 4.9 and 4.10. The PEG contents vary from 1 to 17%. If the doping content is increased more than 17%, then the film becomes extra fluidic and then there will be no well-defined shape and consistency of the film. Also, it has to be noticed that, in Figure 4.9, when the film is not doped with PEG, the optical activity starts only at a higher pressure. We can

observe that if a pressure of 1.6×10^4 psi is applied to the film without the doping, the coupling peak will be shifted to around 583 nm. But, if the film is doped with 17% PEG, then with only 1/10 amount of pressure, the peak is shifted to 577 nm.
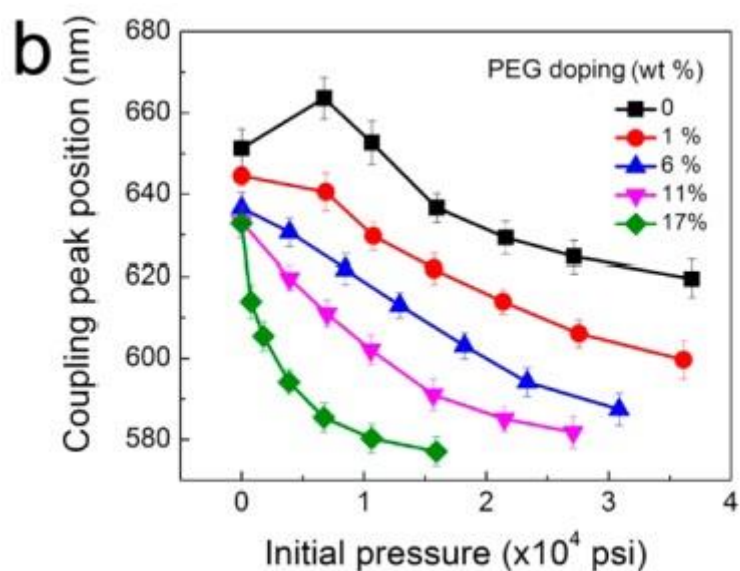
Figure 4.9 Plot of pressure-dependent coupling peak shift for films doped with different amounts of PEG (press time is 1 min).

Source: Colorimetric Stress Memory Sensor Based on Disassembly of Gold Nanoparticle Chains by Xiaogang Han, Yiding Liu and Yadong Yin
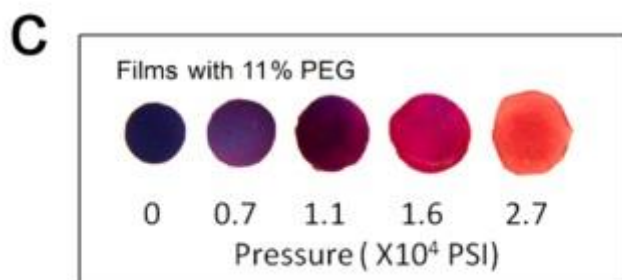
Figure 4.10 Digital images of films doped with 11 wt % PEG after experiencing different pressures for 1 min.

Source: Colorimetric Stress Memory Sensor Based on Disassembly of Gold Nanoparticle Chains by Xiaogang Han, Yiding Liu and Yadong Yin

Not only the disassembly increases with the doping, but also the sensitivity of deformation and this can be seen in Figure 4.11. Along with it, it has to be noticed that even the coupling peak shifts with the amount of PEG. With similar shift in the peak, the deformation was also found to be of the same extent. This was unique because it is

related to different amount of PEG loadings. Thus, with different amount of PEG loadings, if the shift in peaks are the same, then even their deformations will be the same.
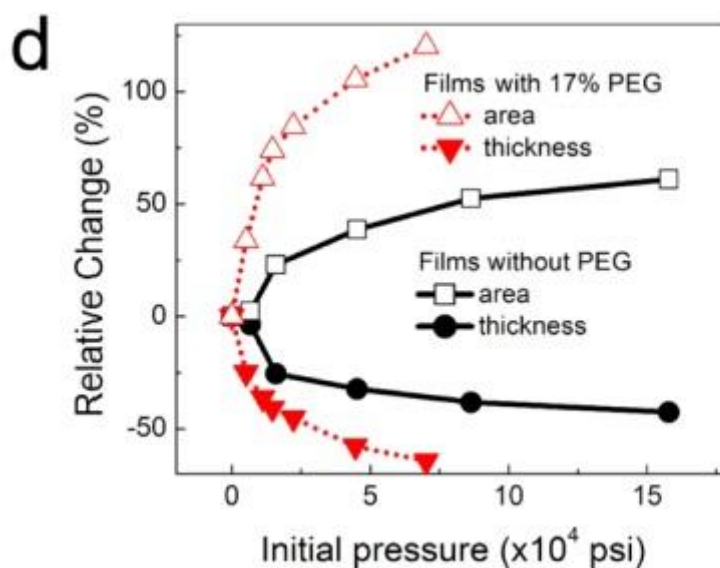
Figure 4.11 Deformation profiles of films without and with 17 wt % PEG doping under different pressures for 1 min.

Source: Colorimetric Stress Memory Sensor Based on Disassembly of Gold Nanoparticle Chains by Xiaogang Han, Yiding Liu and Yadong Yin

When investigated, the film without PEG doping underwent a 61% expansion in area and a plasmonic shift to 583 nm after experiencing 1.6×10^5 psi of pressure, while the one doped with 17 wt % of PEG showed a 66% change in area and a plasmonic shift to 577 nm after being subjected to 1.6×10^4 psi of pressure. This fulfils the relation of extent of disassembly equivalent to the extent of film deformation. Thus, with the amount of plasticizer, polymer films with different degree flexibility can be made to detect a wide range of stresses by outputting optical responses.

CHAPTER 5

STUDY AND ANALYSIS OF SILVER NANOPARTICLES

5.1 Extinction Profile of Silver Nanoparticle Array

5.1.1 Silver Nanoparticle Size and Absorbance Spectra Characteristics

Extinction profiles describe how light or radiation would interact when incident upon matter. When radiation interacts with matter, it first undergoes absorption and then it might emit the same light. Both these processes are different and they depend on the material. The combined effect of this absorption and scattering of light can be understood by the extinction coefficient.

In case of silver nanoparticle, it is the size that will decide how the profile is formed. Figure 5.1 shows two different Ag NP sizes and how the extinction profiles differ. Figure 5.2 shows many other sizes of Ag NP and we can see that the wavelength increases with increase in size. Volumetric cross-section is the key part when it comes to silver nanoparticles. To support this, if any two sizes of AgNPs are selected and with their help, we populate the given volume, then the extinction spectra will be seen to have a dominating effect by the larger size of the particles.
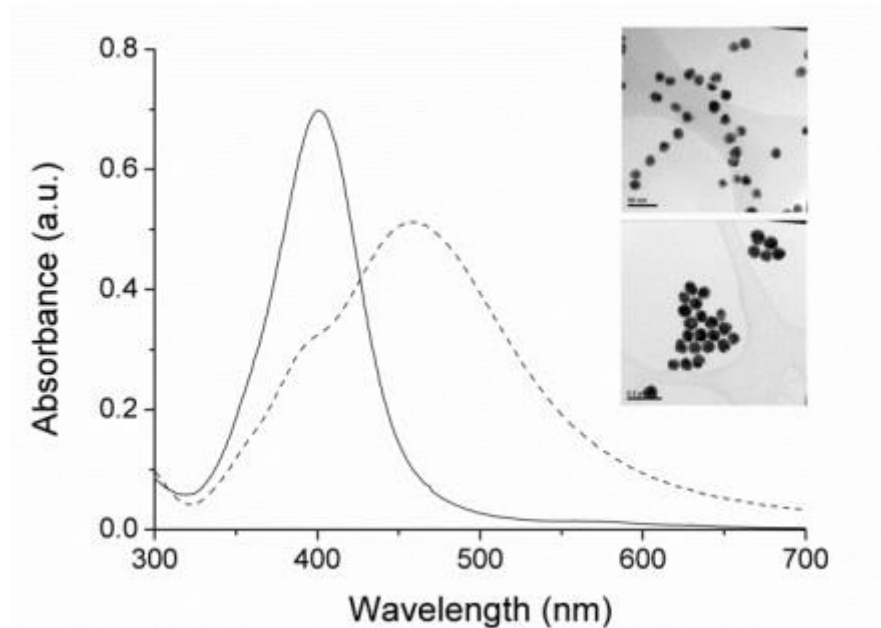
Figure 5.1 3 UV-visible spectra and example HR-TEM images of 19.0 nm (solid line and upper image) and 74.8 nm (dashed line and lower image) citrate-capped silver nanoparticles.

Source: Rapid method to estimate the concentration of citrate capped silver nanoparticles from UV-visible light spectra D. Paramelle, A. Sadovoy, S. Gorelik, P. Free, J. Hobley, and D. G. Fernig
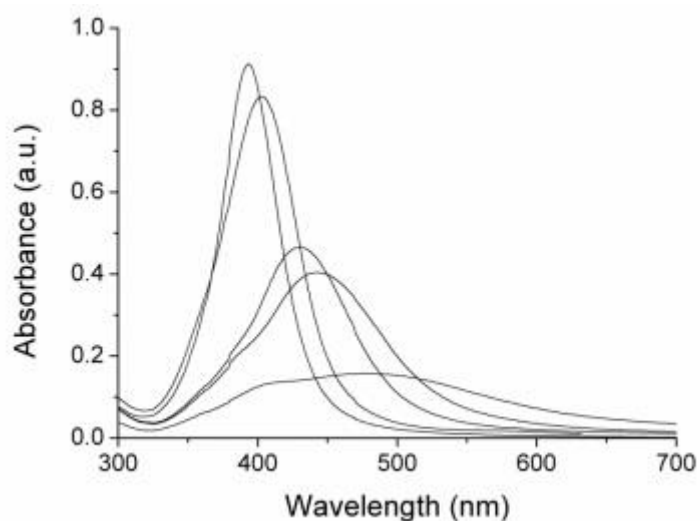
Figure 5.2 Exemplar UV-visible spectra of citrate-capped silver nanoparticles. Diameters of nanoparticles (expressed as %volume distribution, determined by HR-TEM) in increasing wavelength of λmax are: 19.0 nm, 30.4 nm, 57.0 nm, 64.1 nm, and 95.3 nm, respectively.

Source: Rapid method to estimate the concentration of citrate capped silver nanoparticles from UV-visible light spectra by D. Paramelle, A. Sadovoy, S. Gorelik, P. Free, J. Hobley and D. G. Fernig

Apart from the particle size, even the scattering of extinction coefficients plays a vital role in obtaining the final extinction profile. In order to get the value of absorbance,

we use Beer Lambert law and if the sample is diluted, then the result fits accurately in the case of Ag NP. The effect of scattering and absorbance will have the same effect at particle size of 52 nm. [29]

The experiments were conducted to measure spectra, at size 50 nm and lower, in order to define optimal concentrations of a given sample with different dilutions. This series of tests were compared with simulated absorbance and the result is shown in Figure 5.3.
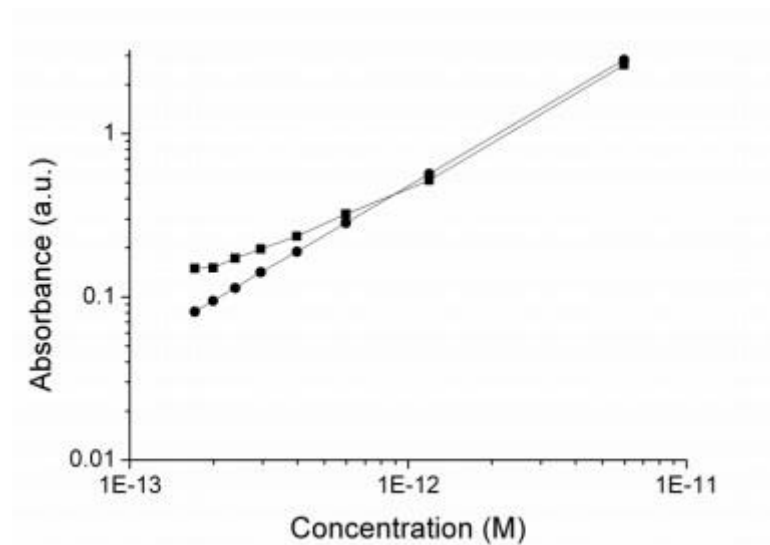
Figure 5.3 Comparison between intensity of maximum absorbance of solutions at different concentrations for measured (black squares) and simulated (black circles) absorbance for 45.9 nm nanoparticles.

Source: Rapid method to estimate the concentration of citrate capped silver nanoparticles from UV-visible light spectra by D. Paramelle, A. Sadovoy, S. Gorelik, P. Free, J. Hobley, and D. G. Fernig

We can see from the Figure 5.3, that the point at which absorbance intensity for the maximum peak overlaps is between 0.3 and 0.4. So, this is the range in which the calculations and measurement of absorbance were carried out. The size is restricted to 50 nm or lower because as the size keeps on increasing, the scattering effect becomes more prominent.

The tests were also carried out for larger Ag NPs to understand the effects of a wide range of Ag NP sizes. It was found out that the closeness of the absorbance and fitting curve of diluted Ag NP solution was found to be below 0.3 but it was not as accurate as it was found in terms of sizes below 50 nm. Thus, if we are interested in Ag NPs with a size larger than 50 nm, then the absorbance value has to be chosen to be equal to ~0.3. The validation of this concept is explained below and the results have been used from the literature. [29]

Using 50 nm and 80 nm silver nanoparticles, the spectrometer (Molecular Probes Spectramax 384) absorbance (below 0.3) was validated against two other spectrometers; Shimadzu UV-3600 (2nm slit width) and Ocean Optics USB-4000 (no slit setting, but with a resolution of 1.5 nm/pixel). Five different samples, prepared on different days, gave an absorbance S.D. of 5.8%. Using the Spectramax 384 for calibration of Methylene Blue in water gave a peak extinction coefficient of (7.34 ± 0.11) x 104 M^{-1} cm^{-1} from three separate dilutions; these are comparable to the average values from of a range of literature. [30] – [33]

5.1.2 Scattering from One-dimensional and Two-dimensional Arrays

The inter-particle spacing plays a crucial role in determining the outcome of the interaction. While considering 1D or 2D arrangement, there will be considerable amount of electromagnetic coupling between the particles over the complete array. The other factors that has an influence over the spectra are, coupling interactions and polarization of the incident light. [34] - [38]

We discuss the near field and far field plasmon effects and how the particle spacing dictates the results. In Ag NP, it causes a significant variation in terms of optical response and it is also due to the dipole orientation in the population. If the coupling is

due to parallel but non-collinear dipoles, then there will be a blue-shift in the plasmon wavelengths, whereas if the dipoles are parallel and collinear, then it will be red shifted.

This analysis is directed towards getting a better candidate in terms of chromic response so that the sensors are designed accordingly. Thus, for 2D arrays, we have to consider dipole interactions which leads to red shift due to the resonance. [39] But, the usual norm breaks in terms of electrostatics when we think of an arrangement when the particle spacing exceeds 70 nm. In this case, the long range electrodynamic interactions take over. This knowledge helps in designing the array structure so that the spectra is directly influenced by this array and the detection can be applied according to the specific range.

In order to design array and structures, several numerical methods have been developed. These methods include the following: the discrete dipole approximation (DDA) [40] [41], the multiple multipole method (MMP), [42] the finite difference time domain method (FDTD) [43] and the T-matrix method [44]. The details of the method are described below. [45]

The DDA method (also called the volume discretization method) divides the object into a large number of polarizable cubes. The induced dipole polarizations in these cubes are determined self consistently, and then, the optical properties are determined using the induced polarizations. The MMP method separates the field domain into a number of subdomains and then solves the differential equations in each subdomain analytically and matches the boundary conditions between different domains numerically, that is, via least-squares fitting.

FDTD methods discretize the entire volume of the scatterer to numerous Yee cells and then solve Maxwell's equations as a function of time numerically. The T-matrix method expresses the fields inside and outside the object as expansions in vector spherical harmonics and then does exact matching within the subspace of the spherical

harmonic basis by projecting the matching equations onto the basis. These numerical methods have enabled the computations of surface plasmon resonances for complex geometrical configurations and the inclusion of particle interactions at a high level. [46] [47]

The literature further elaborates the numerical methods and the electrodynamic model to obtain the extinction spectra. Also, the geometrical clusters were established on the basis of numerical simulations in terms of infinite two-dimensional arrays. [45] But, in this thesis, the focus will be on analysing the results gathered from the calculations and will be interpreted in current application. To compare the results, the calculations are just based on T-matrix and coupled dipole methods to get the extinction spectra for both the types of arrangement.

The result is for silver nanoparticles with a radius of 5 and 30 nm and are spherical in shape. Array spacing is of prime importance on which the results have been established. According to it, if the spacing D/2r is greater than unity, the spectra of the array described by the dipole approach can be described accurately. As the spacing approaches unity, the results improve and this can be achieved by choosing the array dimensions to be smaller. The study in this research mainly involved variation of dipole plasmon resonance wavelength and width by virtue of examining various particle size, array spacing, array symmetry and polarization direction.

For one-dimensional array, if the polarization is perpendicular, the wavelength blue shifts and in case of parallel arrangement, the wavelength red shifts. But, the width of the extinction spectra spreads out in case of both perpendicular and parallel polarization. [45] It has been stated that, blue shift in this case is not important.
In case of 2D array, if the spacing is greater than 75 nm and the polarization is parallel, the plasmon resonance blue shifts. This is because the array spacing decreases in that

case. But, if the spacing between particles is smaller than 75 nm, the plasmon resonance red shifts.

Apart from spacing, even the density carries significant importance in determining the plasmon peak and extinction spectra. The spectra spread out if the density is increased for spacing smaller than 180 nm, while the peak is sharper for the spacing greater than 180 nm. The square or hexagon or any other symmetry does not dictate the change in array spectrum.

The data for all the above observations has been shown below in the form of various plots. This includes all the changes that resulted from changing particle size, densities, blue shift and red shift. All the data has been assumed to be accurate and the necessary predictions will be made based on the data given in other reference. [45]
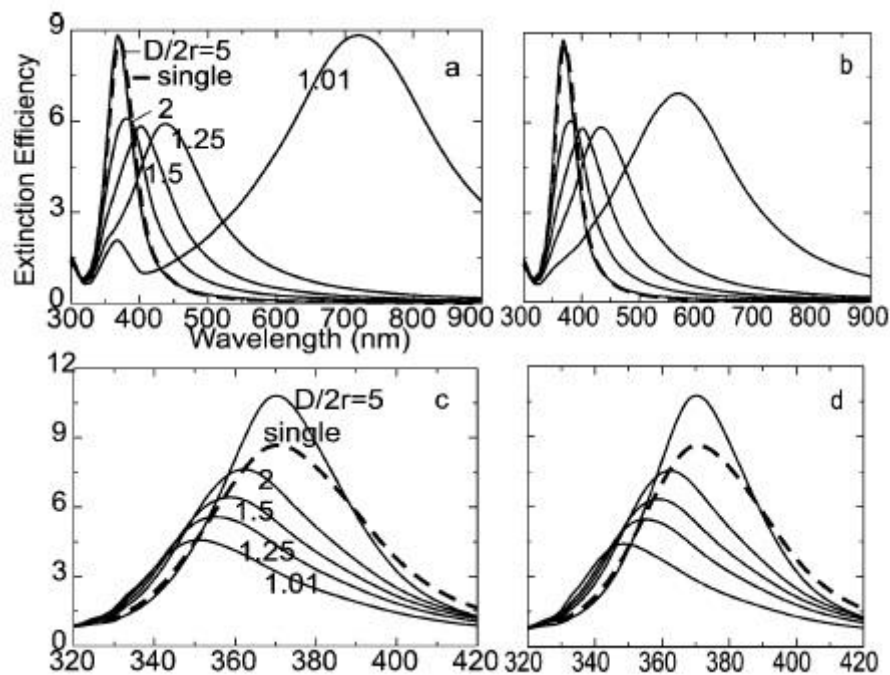
Figure 5.4 Variation of extinction spectrum for linear chain of 30-nm spheres with $D/(2r)$ chosen to be 5, 2, 1.5, 1.25, and 1.01: (a) T-matrix results for parallel polarization; (b) CD results for parallel polarization; (c) T-matrix results for perpendicular polarization; (d) CD results for perpendicular polarization. Also included in each plot is the result for a single sphere
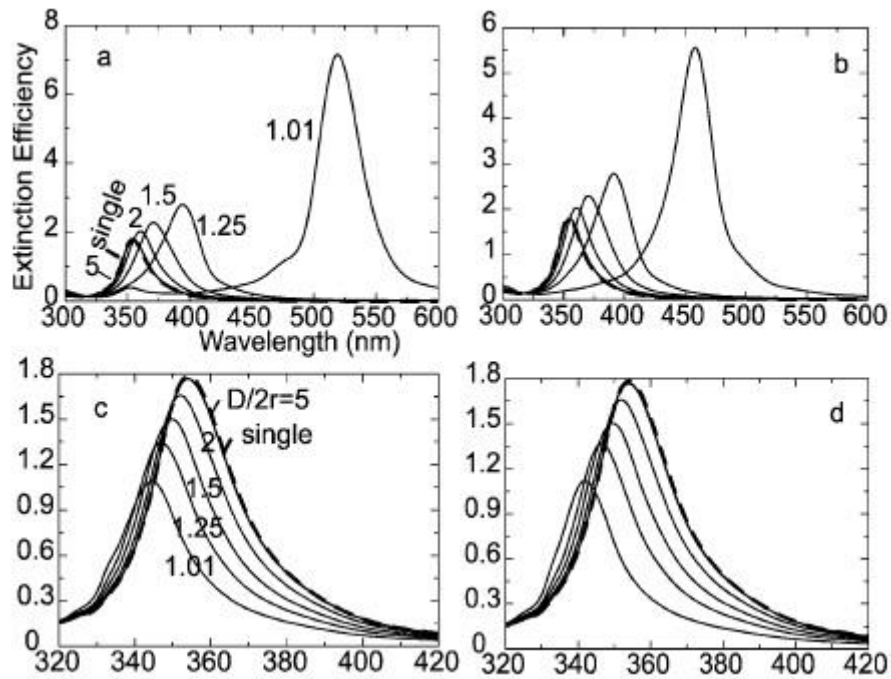
Figure 5.5 Variation of extinction spectrum for linear chain of 5-nm spheres with $D/(2r)$ set to be 5, 2, 1.5, 1.25, and 1.01: (a) T-matrix results for parallel polarization; (b) CD results for parallel polarization; (c) T-matrix results for perpendicular polarization; (d) CD results for perpendicular polarization. Also included in each plot is the result for a single sphere.
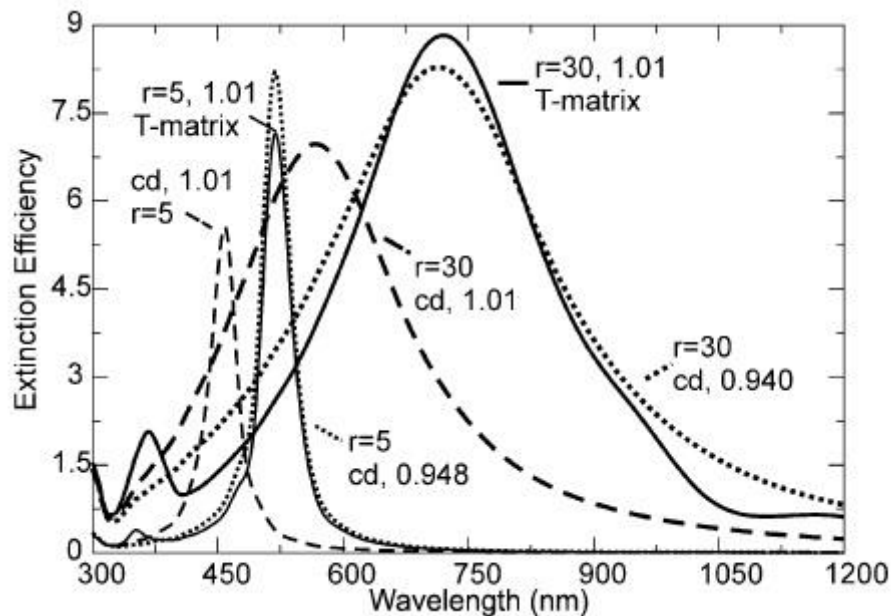
Figure 5.6 Extinction of one-dimensional chain using CD approach to simulate T-matrix multipole results for $D/(2r)$) 1.01 with r) 30 and 5 nm.
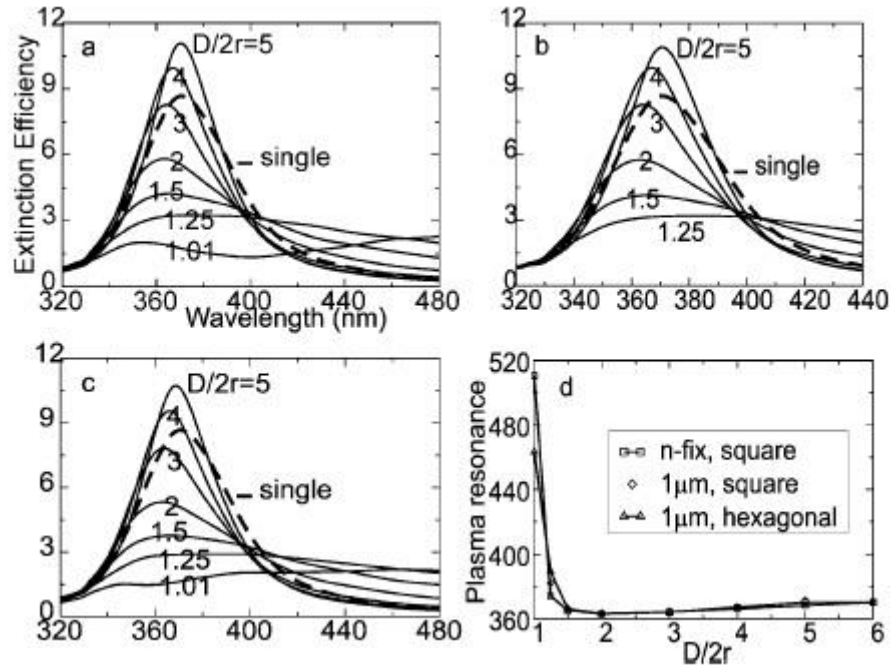
Figure 5.7 Variation of extinction for two-dimensional array of 30-nm spheres with different $D/(2r)$ obtained from T-matrix multipole calculation: (a) results for square structure, N fixed; (b) results for square structure, fixed array size; (c) results for hexagonal structure, fixed array size; (d) comparison of $\imath$max obtained for these three structures. Also included in each plot is the result for a single sphere. Note that a different wavelength scale is used in panels a-c.

The above stated optical behaviour for 2D array, based on the numerical methods and comparison with simulations, showed that blue shifts are due to the long range radiative dipolar coupling. Also, sharp peaks are observed for large spacing in this case. Red shifts in plasmon coupling is due to the short range dipolar coupling, along with the broadening of the spectra for small spacing.

Finally, the optimal blue shifts and narrowing are found when the array spacing is slightly smaller than the plasmon wavelength, while red shifts and broadening can be found for spacing much smaller than the plasmon wavelength. The $1/r$ term plays a less important role for one dimensional chains, and as a result, the plasmon wavelength shows a monotonic dependence on array spacing.

The shape of the nanoparticle also exhibits peak in different regions and depending on the target region (in our case visible region), we can use different sizes

and shapes of Ag NPs. Figure 5.8 shows the plots of UV-vis spectra of different combinations of size and shape. [48]
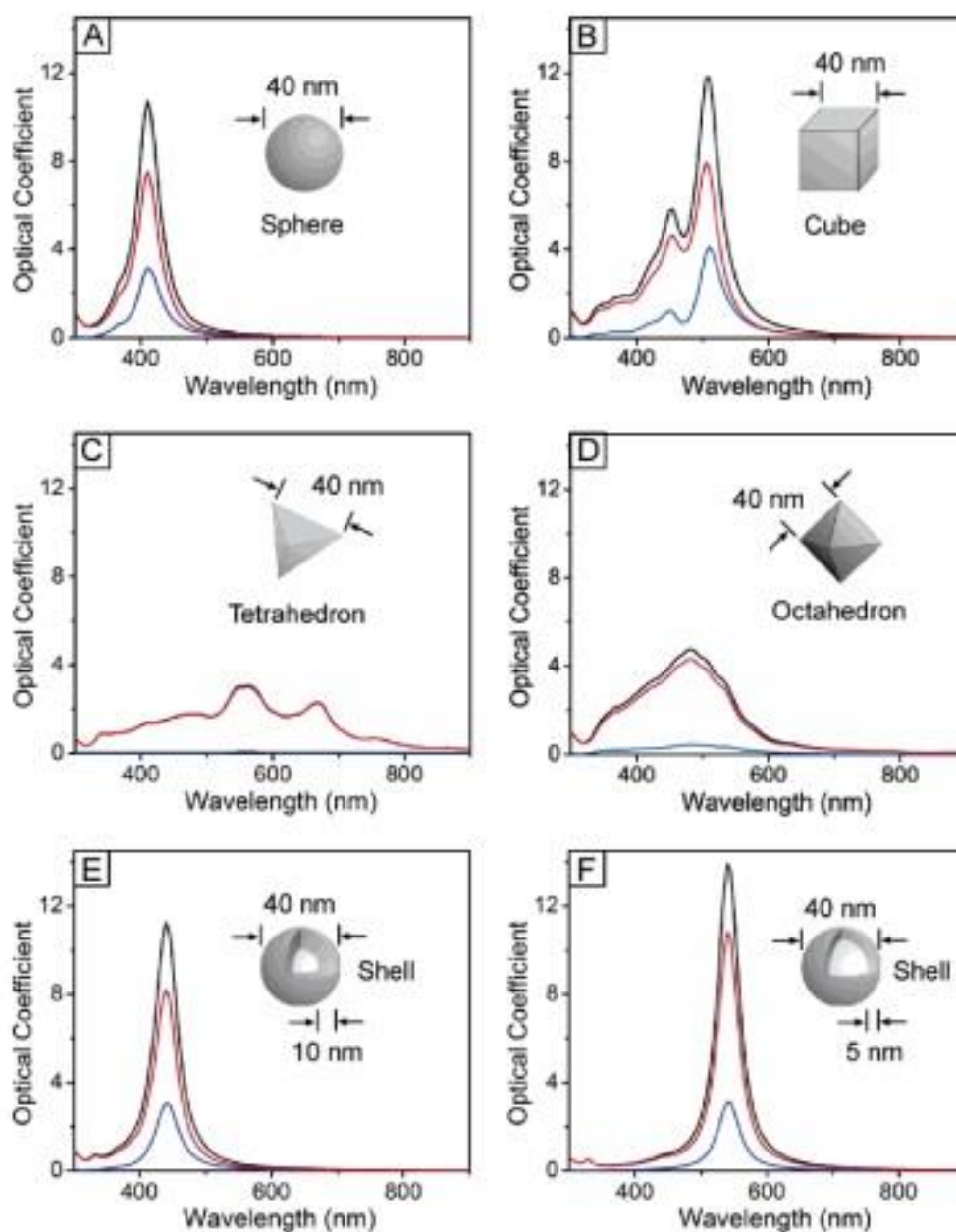
Figure 5.8 Calculated UV-vis extinction (black), absorption (red), and scattering (blue) spectra of silver nanostructures, illustrating the effect of a nanostructure's shape on its spectral characteristics. An isotropic sphere (A) exhibit spectra with a single resonance peak. Anisotropic cubes (B), tetrahedra (C), and octahedra (D) exhibit spectra with multiple, red-shifted resonance peaks. The resonance frequency of a sphere red-shifts if it is made hollow (E), with further red-shift for thinner shell walls (F).

5.2 Comparison of Various Data Between Ag NPs and Au NPs

The UV-vis absorption spectra of gold and silver nanoparticles, of an aqueous solution using sodium acrylate, have been compared and shown in Figure 5.9.
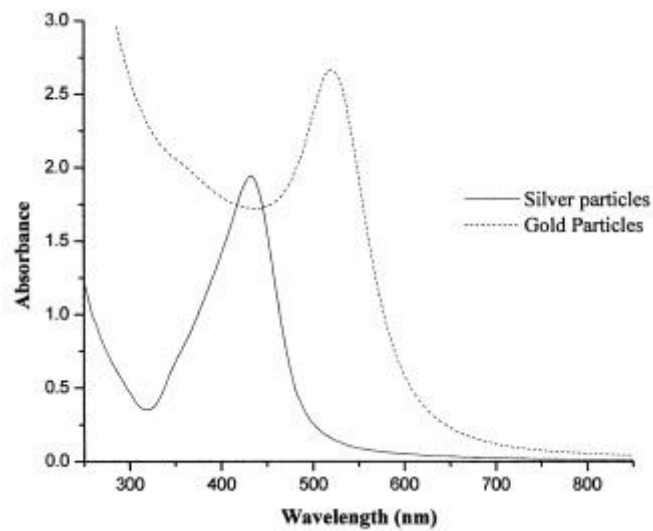
Figure 5.9 UV-visible absorption spectrum of an aqueous solution of gold and silver nanoparticles formed using sodium acrylate (SA).

Source: Preparation of Acrylate-Stabilized Gold and Silver Hydrosols and Gold-Polymer Composite Films by Irshad Hussain, Mathias Brust, Adam J. Papworthcand Andrew I. Cooper.

The comparison of AuNP-PVP and AgNP-PVP has been shown in Figure 5.10

and 5.11.
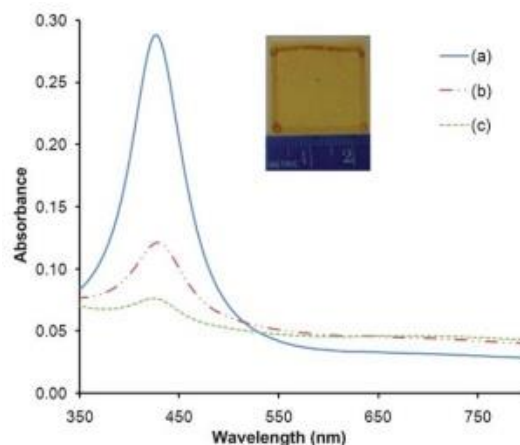
Figure 5.10 Solid state UV-vis spectra of the AgNPs–PVP nanocomposite films with weight ratios of AgNO3 to PVP, [AgNO3/PVP] ¼ (a)1 : 3.5, (b) 1 : 7, and (c)1 : 14. The inset shows the typical optical image of AgNPs–PVP nanocomposite film on slide glass.

Source: Polymer-assisted preparation of metal nanoparticles with controlled size and morphology by Sea-Ho Jeon, Ping Xu, Bin Zhang, Nathan H. Mack, Hsinhan Tsai, Long Y. Chiangb and Hsing-Lin Wang
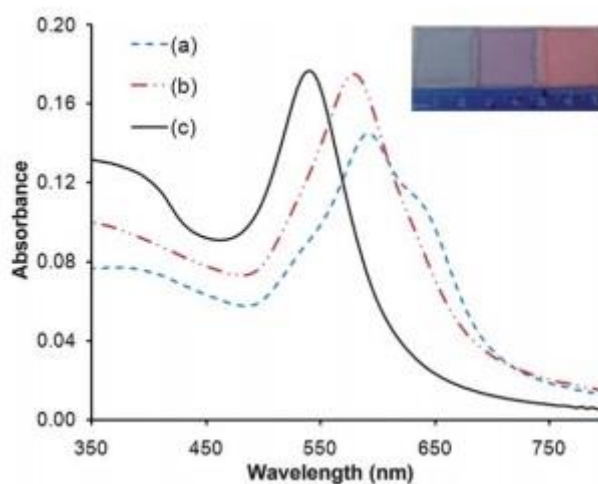
Figure 5.11 Solid state UV-vis spectra of the AuNPs–PVP nanocomposite films with weight ratios of HAuCl4 to PVP, [HAuCl4/PVP] ¼ (a) 1 : 1.5, (b) 1 : 2, and (c) 1 : 4. The inset shows the optical images of AuNPs–PVP nanocomposite films on slide glasses. From the left side, optical images corresponding to (a), (b), and (c).

Source: Polymer-assisted preparation of metal nanoparticles with controlled size and morphology by Sea-Ho Jeon, Ping Xu, Bin Zhang, Nathan H. Mack, Hsinhan Tsai, Long Y. Chiangb and Hsing-Lin Wang.

Figure 5.12 shows the effect of temperature on AgNP and its extinction profile.
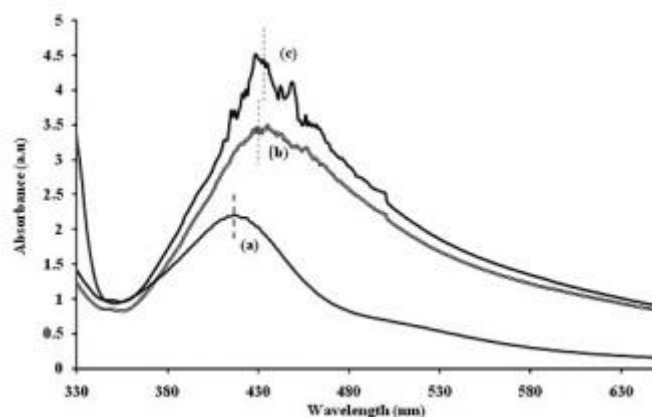
Figure 5.12 UV-Visible absorption spectra of silver nanoparticles at various reactant temperatures:(a) 808C, (b) 1008C and (c) 1208C.

Source: Optical and thermodynamic studies of silver nanoparticles stabilized by Daxad 19 surfactant by Nurul Akmal Che Lah, Mohd Rafie Johan.

Apart from the observations above, other references from the literature were also used to validate these results and to analyse how closer are the values for absorbance peaks. Plots were analysed from other materials and the data were acquired. This is shown in Table A1 in the Appendix A. [28] The difference in the obtained results have been shown in Figures 5.13 and 5.14. In all the analysis done until now, this holds utmost importance as it shows the value of absorbance peak with respect to the diameter. The size plays an important role since for designing sensors, it becomes important to know the size that is appropriate for a given product.

Figure 5.13 Absorbance peaks for silver nanoparticles obtained experimentally (empty circles), manufacturer supplied information (black triangles) and simulated (empty squares) are shown. x-error is the S.D. of the diameter.
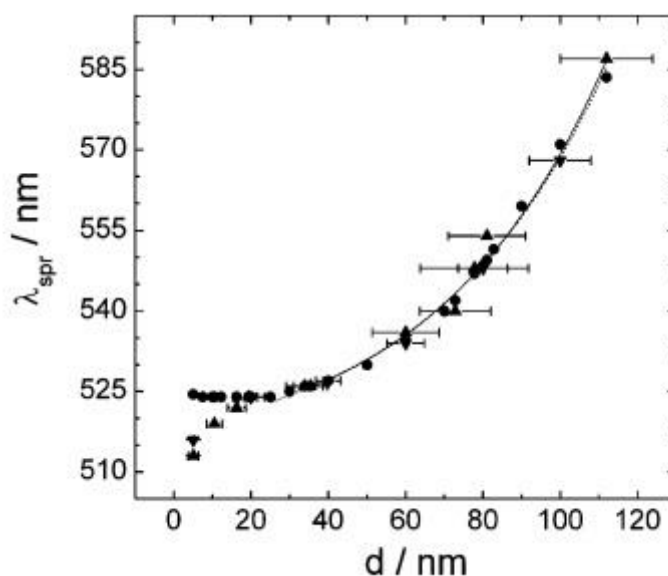
Figure 5.14 Position of the surface plasmon resonance peak (λspr) as a function of the particle diameter for AuNPs in water: calculated (circles); experimentally measured (downward pointing triangles, commercial AuNPs; upward-pointing triangles, in house synthesized AuNPs). An exponential fit to the theoretical (experimental) data for d > 25 nm is shown as a dotted (dashed) line.

CHAPTER 6

CONCLUSIONS AND RECOMMENDATIONS

This analysis is based on the application of optical properties of metal nanoparticles in sensor technology. The concept behind this application is that when pressure is applied on a film, which is designed with the help of nanoparticles, it can be measured or observed visually by realising the colour change of the film. Silver and gold nanoparticles have been used to produce new classes of chemical, biological and optical sensors, in which aggregation – induced electromagnetic interactions between the particles results in colour change that signals detection.

This thesis has been structured in a way that a rigorous study on Au NPs has been done by reviewing the literature and analysing the data. The data were studied in order to understand the factors which play a major role in developing this technology. After understanding the concept behind the technology, an analysis of silver nanoparticles was conducted. This analysis included details that would be needed to understand whether or not the particle fulfils the basic criteria. Particle size, shape, density, spectral characteristics, effect of temperature, particle spacing, polymer material and all related properties were studied in terms of Ag NPs; the results were then compared with that of already existing technology and particles used for it, i.e. Au NPs.

The aim of this study was to know whether or not, silver nanoparticle is a better and suitable candidate for sensor applications in terms of usability, expense, market requirements and production.

Silver has many advantages over gold in terms of usability, costing and its effect on environment and humans. For the same reason, silver nanoparticles are extensively used in medical applications because they have a high surface area per unit mass. There will be a release of silver ions in the environment continuously because of its surface

area and as they are bioactive, they have various antimicrobial properties against bacteria. We can develop applications of wide range of silver ion profiles, by controlling the size, shape, surface and agglomeration state of nanoparticles. The optical properties, high electrical conductivity and the antimicrobial properties are the main reason for silver nanoparticles to be one of the most commonly used particles.

The difference becomes visible in terms of LSPRs of Ag NP which shows a better response. They can be tuned from 380 nm in the Ultra Violet to Infrared at 6000 nm by only varying size and shape with the maxima of triangles, blunted triangles and hemispheres of comparable sizes at 623, 532 and 432 nm, respectively. Also we observed that the gold nanoparticle has to be of very specific size so that the plasmon peak falls in the visible region. For example, gold nanoparticles of 20nm spheres have their LSPR peak at 520 nm which is of red colour.

In a nutshell, a stress-responsive colorimetric film that can memorize stress was studied using AuNPs. Plasmonic shift caused by disassembly of nanoparticle chains emits light which is in the visible region. Disassembly was a result of the deformation of the polymer on which it has been casted. The deformation is inelastic and thus it never returns to its original form and thus the stress experienced by the film remains as it is and the colour imparted during the plasmonic shift stays as it is. The major target of the thesis was to see if the AgNPs can replace AuNPs and after detailed comparison and analysis, the use of AgNPs looks much more promising and it should be a major area of research to exploit the advantages of silver nanoparticles.

APPENDIX A

SILVER NANOPARTICLES
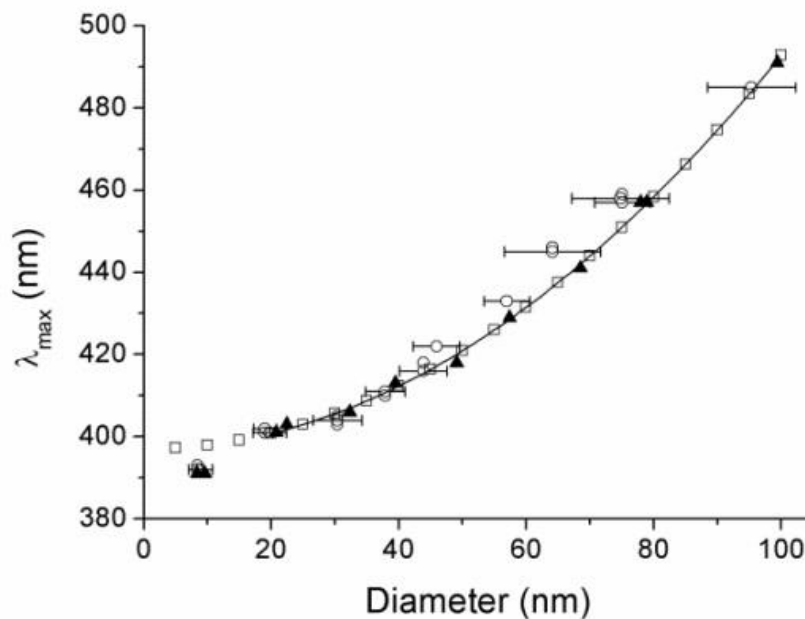
Absorbance peaks for silver nanoparticles obtained experimentally (empty circles), manufacturer supplied information (black triangles) and simulated (empty squares) shown in the table below.

Table A.1 Data of Experimental, Manufacturer and Simulated

Experimental		Manufacturer		Simulated	
Diameter	**Wavelength**	**Diameter**	**Wavelength**	**Diameter**	**Wavelength**
8.88853	390.839	8.3879	393.548	5.16289	397.032
20.749	400.903	18.768	401.29	9.86506	397.419
22.4776	402.839	30.1485	404	14.8132	398.581
32.3722	405.935	37.5615	410.194	24.9529	402.839
39.5361	412.903	43.7336	417.935	29.4027	405.548
48.9317	417.935	45.9534	421.806	34.8419	408.645
57.3243	429.161	56.5738	433.032	44.7269	416.387
68.1907	441.161	63.7256	445.806	50.1645	420.258
77.5639	457.032	74.5936	457.032	54.8579	424.903
78.3057	457.419	74.5896	458.968	59.7948	431.484
98.7807	491.097	94.8315	485.677	64.7317	438.065
				69.6702	443.871
				74.6072	450.452
				79.2934	458.581
				84.7229	466.323
				89.4075	475.226
				94.5888	483.355
				99.5193	493.032

GOLD NANOPARTICLES

Position of the surface plasmon resonance peak (λspr) as a function of the particle diameter for AuNPs in water: calculated (circles); experimentally measured (downward pointing triangles, commercial AuNPs; upward-pointing triangles, in house synthesized AuNPs) shown in the table below.

Table A.2 Data of Experimental, Manufacturer and Simulated

Experimental		Manufacturer		Simulated	
Diameter	**Wavelength**	**Diameter**	**Wavelength**	**Diameter**	**Wavelength**
4.57249	524.754	5.09294	516.163	5.09294	513.176
7.17472	524	30.5948	525.058	10.8178	519.135
10.2974	523.992	39.9628	526.526	16.0223	521.736
12.8996	523.985	60.7807	533.94	60.2602	535.808
16.0223	523.976	80.5576	547.704	73.2714	539.508
19.6654	523.967	100.855	567.816	81.5985	554.05
24.8699	523.953			112.825	586.83
30.5948	524.684				
34.7584	525.42				
36.3197	525.789				
39.9628	526.9				
50.3717	529.86				
60.7807	535.06				
70.1487	539.516				
73.2714	541.749				
78.4758	547.337				
80.0372	547.706				
81.0781	548.823				
81.5985	549.569				
83.1599	551.059				
90.4461	559.628				
100.335	570.805				
112.305	583.097				

Table A.3 Geometric, Extinction, Absorption, and Scattering Cross Sections and Efficiencies for 16 Different Sizes of Silver Nanoparticles

mean diameter (nm)	geometric cross section (10¹¹ cm²)	extinction cross section (10¹¹ cm²)	extinction efficiency	absorption cross section (10¹¹ cm²)	absorption efficiency	scattering cross section (10¹¹ cm²)	scattering efficiency
29 ± 3	0.65 ± 0.00	3.13 ± 0.46	4.8 ± 1.2	2.91 ± 0.47	4.5 ± 0.7	0.29 ± 0.05	0.5 ± 0.1
34 ± 3	0.90 ± 0.00	3.77 ± 0.24	4.2 ± 0.7	3.00 ± 0.27	3.3 ± 0.3	0.73 ± 0.07	0.8 ± 0.1
36 ± 3	1.04 ± 0.01	5.53 ± 0.60	5.3 ± 1.1	4.81 ± 0.60	4.6 ± 0.6	0.68 ± 0.09	0.7 ± 0.1
44 ± 3	1.50 ± 0.01	8.47 ± 0.48	5.7 ± 0.9	6.28 ± 0.53	4.2 ± 0.4	2.42 ± 0.20	1.6 ± 0.1
48 ± 3	1.82 ± 0.01	17.23 ± 0.37	9.5 ± 1.2	11.79 ± 0.78	6.5 ± 0.4	5.85 ± 0.39	3.2 ± 0.2
52 ± 3	2.12 ± 0.01	17.43 ± 0.47	8.2 ± 1.0	8.12 ± 0.56	3.8 ± 0.3	8.18 ± 0.56	3.9 ± 0.3
59 ± 3	2.70 ± 0.07	22.54 ± 2.55	8.4 ± 1.3	10.52 ± 1.36	3.9 ± 0.5	12.82 ± 1.66	4.8 ± 0.6
61 ± 3	2.96 ± 0.04	30.94 ± 1.44	10.5 ± 1.2	13.17 ± 1.03	4.5 ± 0.4	18.70 ± 1.46	6.3 ± 0.5
76 ± 3	4.53 ± 0.19	34.91 ± 4.27	7.7 ± 1.2	12.92 ± 1.78	2.9 ± 0.4	23.14 ± 3.18	5.1 ± 0.7
78 ± 4	4.77 ± 0.12	37.71 ± 2.50	7.9 ± 0.9	13.17 ± 1.20	2.8 ± 0.3	30.79 ± 2.80	6.5 ± 0.6
92 ± 5	6.69 ± 0.11	49.36 ± 1.71	7.4 ± 0.8	18.47 ± 1.32	2.8 ± 0.2	38.61 ± 2.75	5.8 ± 0.4
96 ± 3	7.31 ± 0.04	53.66 ± 0.57	7.3 ± 0.5	17.30 ± 1.10	2.4 ± 0.2	46.14 ± 2.92	6.3 ± 0.4
105 ± 4	8.63 ± 0.50	59.62 ± 5.80	6.9 ± 0.9	22.22 ± 2.57	2.6 ± 0.4	50.54 ± 5.85	5.9 ± 0.8
113 ± 3	10.07 ± 0.05	66.38 ± 0.53	6.6 ± 0.4	23.41 ± 1.48	2.3 ± 0.2	58.95 ± 3.71	5.9 ± 0.4
120 ± 4	11.24 ± 0.16	77.24 ± 1.47	6.9 ± 0.4	27.21 ± 1.78	2.4 ± 0.2	69.63 ± 4.55	6.2 ± 0.4
136 ± 5	14.62 ± 1.16	95.43 ± 10.08	6.5 ± 0.9	33.54 ± 4.10	2.3 ± 0.4	85.15 ± 10.40	5.8 ± 0.9

APPENDIX B

MATLAB PROGRAMS FOR CWT

Program B.1 Determination of Analytical Scale Number (Q)

```
[m,I]=size(x);

for p=1:m

Abs=x(p,:);

y=detrend(Abs);

i=0;

n=401;

for j=1:n

while y(1,j)+i<0

i=i+0.01;

end

end

y=y+i;

for q=1:16

a=cwt(y,1:q*4,'mexh');

b=sum(a);

i=0;

n=401;

for j=1:n

while b(1,j)+i<0

i=i+0.01;

end

end
```

```
b=b+i;

subplot(4,4,q)

plot(w,b)

end

if p>=m

p

break

else p

pause

end

end
```

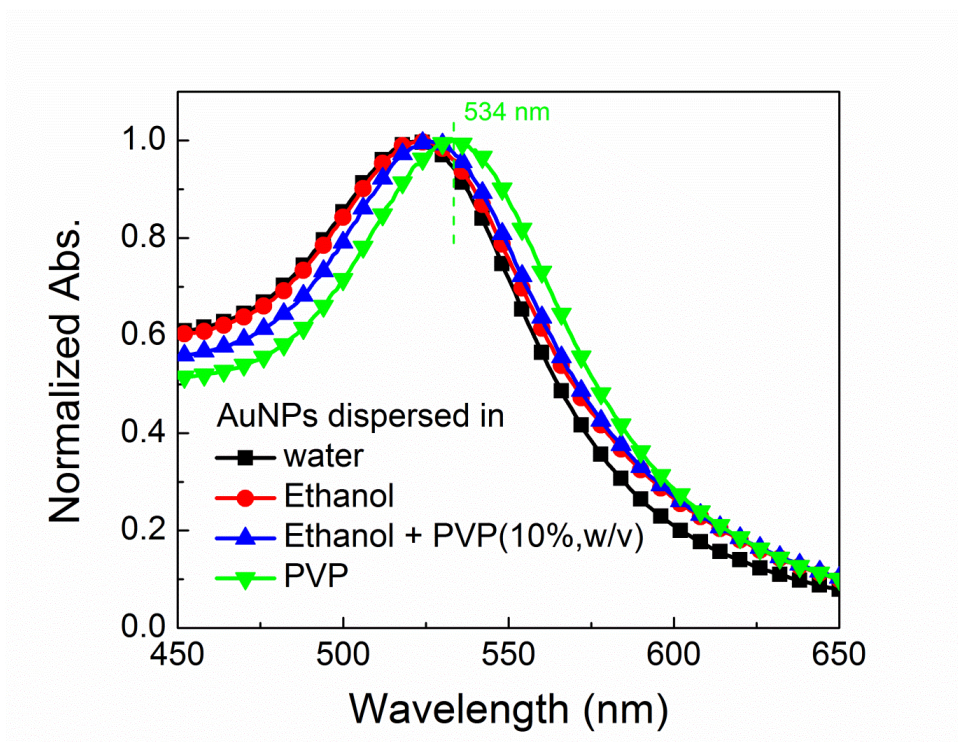**Program B.2** Spectrum Transformation and its plot at the end of the code

```
t=0;

t=x(1,:);

[m,I]=size(x);

for r=1:m;

Abs=x(r,:);

y=detrend(Abs);

i=0;

n=401;

for j=1:n

while y(1,j)+i<0

i=i+0.01;

end

end
```

```
y=y+i;

a=cwt(y,1:q*4,'mexh');

b=sum(a);

i=0;

n=401;

for j=1:n

while b(1,j)+i<0

i=i+1;

end

end

b=b+i;

t(r,:)=b';

end

t'

plot(w,t)
```

REFERENCES

1) Han, X., Liu, Y., & Yin, Y. (2014). Colorimetric Stress Memory Sensor Based on Disassembly of Gold Nanoparticle Chains. *Nano Letters, 14*(5), 2466-2470. doi:10.1021/nl500144k

2) https://en.wikipedia.org/wiki/Viscoelasticity (accessed March 2017)

3) The Newtonian Fluid by José Mª Franco and Pedro Partal

4) Fractional calculus in viscoelasticity: An experimental study by F.C. Meral, T.J. Royston, R. Magin

5) Turkevich, J., Stevenson, P. C., & Hillier, J. (1951). A study of the nucleation and growth processes in the synthesis of colloidal gold. *Discussions of the Faraday Society, 11*, 55. doi:10.1039/df9511100055

6) Turkevich, J. (1985). Colloidal gold. Part II. *Gold Bulletin, 18*(4), 125-131. doi:10.1007/bf03214694

7) Turkevich, J., & Kim, G. (1970). Palladium: Preparation and Catalytic Properties of Particles of Uniform Size. *Science, 169*(3948), 873-879. doi:10.1126/science.169.3948.873

8) Lee, P. C., & Meisel, D. (1982). Adsorption and surface-enhanced Raman of dyes on silver and gold sols. *The Journal of Physical Chemistry, 86*(17), 3391-3395. doi:10.1021/j100214a025

9) Turkevich, J., Stevenson, P. C., & Hillier, J. (1953). The Formation of Colloidal Gold. *The Journal of Physical Chemistry, 57*(7), 670-673. doi:10.1021/j150508a015

10) Han, X., Goebl, J., Lu, Z., & Yin, Y. (2011). Role of Salt in the Spontaneous Assembly of Charged Gold Nanoparticles in Ethanol. *Langmuir, 27*(9), 5282-5289. doi:10.1021/la200459t

11) Liu, Y., Han, X., He, L., & Yin, Y. (2012). Thermoresponsive Assembly of Charged Gold Nanoparticles and Their Reversible Tuning of Plasmon Coupling. *Angewandte Chemie, 124*(26), 6479-6483. doi:10.1002/ange.201201816

12) Jin, R. (2001). Photoinduced Conversion of Silver Nanospheres to Nanoprisms. *Science, 294*(5548), 1901-1903. doi:10.1126/science.1066541

13) Sun, Y. (2002). Shape-Controlled Synthesis of Gold and Silver Nanoparticles. *Science, 298*(5601), 2176-2179. doi:10.1126/science.1077229

14) Gao, C., Vuong, J., Zhang, Q., Liu, Y., & Yin, Y. (2012). One-step seeded growth of Au nanoparticles with widely tunable sizes. *Nanoscale, 4*(9), 2875. doi:10.1039/c2nr30300k

15) Ahmadi, T. S., Wang, Z. L., Green, T. C., Henglein, A., & El-Sayed, M. A. (1996). Shape-Controlled Synthesis of Colloidal Platinum

Nanoparticles. *Science,272*(5270), 1924-1925. doi:10.1126/science.272.5270.1924

16) Boennemann, H., & Richards, R. M. (2010). ChemInform Abstract: Nanoscopic Metal Particles - Synthetic Methods and Potential Applications. *ChemInform,32*(48). doi:10.1002/chin.200148248

17) Puntes, V. F. (2001). Colloidal Nanocrystal Shape and Size Control: The Case of Cobalt. *Science, 291*(5511), 2115-2117. doi:10.1126/science.1057553

18) Cordente, N., Respaud, M., Senocq, F., Casanove, M., Amiens, C., & Chaudret, B. (2001). Synthesis and Magnetic Properties of Nickel Nanorods. *Nano Letters,1*(10), 565-568. doi:10.1021/nl0100522

19) Jin, R. (2001). Photoinduced Conversion of Silver Nanospheres to Nanoprisms. *Science, 294*(5548), 1901-1903. doi:10.1126/science.1066541

20) Henglein, A., & Giersig, M. (2010). ChemInform Abstract: Formation of Colloidal Silver Nanoparticles: Capping Action of Citrate. *ChemInform, 31*(3). doi:10.1002/chin.200003018

21) Beeram, S. (n.d.). The localized surface plasmon resonance (LSPR) response of gold and gold/silver metal nanostructures to protein binding and global refractive index changes. doi:10.18297/etd/94

22) Jeon, S., Xu, P., Zhang, B., Mack, N. H., Tsai, H., Chiang, L. Y., & Wang, H. (2011). Polymer-assisted preparation of metal nanoparticles with controlled size and morphology. *J. Mater. Chem., 21*(8), 2550-2554. doi:10.1039/c0jm02340j

23) Mcfarland, A. D., & Duyne, R. P. (2003). Single Silver Nanoparticles as Real-Time Optical Sensors with Zeptomole Sensitivity. *Nano Letters, 3*(8), 1057-1062. doi:10.1021/nl034372s

24) Uğurlu, G., Özaltin, N., & Dinç, E. (2008). Spectrophotometric Determination of Risedronate Sodium in Pharmaceutical Preparations by Derivative and Continuous Wavelet Transforms. *Reviews in Analytical Chemistry, 27*(4). doi:10.1515/revac.2008.27.4.215

25) Esteban, R., Taylor, R. W., Baumberg, J. J., & Aizpurua, J. (2012). How Chain Plasmons Govern the Optical Response in Strongly Interacting Self-Assembled Metallic Clusters of Nanoparticles. *Langmuir, 28*(24), 8881-8890. doi:10.1021/la300198r

26) Feldstein, M., Shandryuk, G., Kuptsov, S., & Platé, N. (2000). Coherence of thermal transitions in poly(N-vinyl pyrrolidone)–poly(ethylene glycol) compatible blends 1. Interrelations among the temperatures of melting, maximum cold crystallization rate and glass transition. *Polymer, 41*(14), 5327-5338. doi:10.1016/s0032-3861(99)00802-2

27) Jarray, A., Gerbaud, V., & Hemati, M. (2016). Polymer-plasticizer compatibility during coating formulation: A multi-scale investigation. *Progress in Organic Coatings, 101*, 195-206. doi:10.1016/j.porgcoat.2016.08.008

28) Paramelle, D., Sadovoy, A., Gorelik, S., Free, P., Hobley, J., & Fernig, D. G. (2014). A rapid method to estimate the concentration of citrate capped silver nanoparticles from UV-visible light spectra. *The Analyst, 139*(19), 4855. doi:10.1039/c4an00978a

29) Evanoff, D. D., & Chumanov, G. (2004). Size-Controlled Synthesis of Nanoparticles. 2. Measurement of Extinction, Scattering, and Absorption Cross Sections. *The Journal of Physical Chemistry B, 108*(37), 13957-13962. doi:10.1021/jp0475640

30) Bergmann, K., & O'konski, C. T. (1963). A Spectroscopic Study Of Methylene Blue Monomer, Dimer, And Complexes With Montmorillonite. *The Journal of Physical Chemistry, 67*(10), 2169-2177. doi:10.1021/j100804a048

31) Tewari, B., & Boodhoo, M. (2005). Studies in Adsorption: Measurement of External Specific Surface Area of Metal Ferrocyanides by Methylene Blue Dye Adsorption. *Main Group Metal Chemistry, 28*(1). doi:10.1515/mgmc.2005.28.1.23

32) S. Prahl, Oregon Medical Laser Center, Optical Absorption of Methylene Blue, http://omlc.ogi.edu/spectra/mb/ index.html, (Originally accessed May 2014 and accessed again on April 2017)

33) Paramelle, D., Sadovoy, A., Gorelik, S., Free, P., Hobley, J., & Fernig, D. G. (2014). A rapid method to estimate the concentration of citrate capped silver nanoparticles from UV-visible light spectra. *The Analyst, 139*(19), 4855. doi:10.1039/c4an00978a

34) Hövel, H., Fritz, S., Hilger, A., Kreibig, U., & Vollmer, M. (1993). Width of cluster plasmon resonances: Bulk dielectric functions and chemical interface damping. *Physical Review B, 48*(24), 18178-18188. doi:10.1103/physrevb.48.18178

35) Kreibig, U., & Vollmer, M. (1995). Optical Properties of Metal Clusters. *Springer Series in Materials Science*. doi:10.1007/978-3-662-09109-8

36) Quinten, M., & Kreibig, U. (1993). Absorption and elastic scattering of light by particle aggregates. *Applied Optics, 32*(30), 6173. doi:10.1364/ao.32.006173

37) Taleb, A., Petit, C., & Pileni, M. P. (1998). Optical Properties of Self-Assembled 2D and 3D Superlattices of Silver Nanoparticles. *The Journal of Physical Chemistry B, 102*(12), 2214-2220. doi:10.1021/jp972807s

38) Zhao, L., Kelly, K. L., & Schatz, G. C. (2003). The Extinction Spectra of Silver Nanoparticle Arrays: Influence of Array Structure on Plasmon Resonance Wavelength and Width†. *The Journal of Physical Chemistry B, 107*(30), 7343-7350. doi:10.1021/jp034235j

39) Murray, C. A., & Bodoff, S. (1984). Depolarization Effects in Raman Scattering from Monolayers on Surfaces: The Classical Microscopic Local Field. *Physical Review Letters, 52*(25), 2273-2276. doi:10.1103/physrevlett.52.2273

40) Haynes, C. L., Mcfarland, A. D., Zhao, L., Duyne, R. P., Schatz, G. C.,
Gunnarsson, L., . . . Käll, M. (2003). Nanoparticle Optics: The Importance of
Radiative Dipole Coupling in Two-Dimensional Nanoparticle Arrays†. *The
Journal of Physical Chemistry B, 107*(30), 7337-7342. doi:10.1021/jp034234r

41) Okamoto, H. (1996). Improvement of the Discrete Dipole Approximation for the
Scattering Calculations of Clusters: the a 1-Term Method. *The Cosmic Dust
Connection,* 297-301. doi:10.1007/978-94-011-5652-3_22

42) Novotny, L., Pohl, D. W., & Hecht, B. (1995). Scanning near-field optical probe
with ultrasmall spot size. *Optics Letters, 20*(9), 970. doi:10.1364/ol.20.000970

43) Swillam, M. (2013). Finite-Difference Time-Domain Method in Photonics and
Nanophotonics. *Computational Nanotechnology Using Finite Difference Time
Domain,* 1-36. doi:10.1201/b16319-2

44) Scattering By Axisymmetric Particles: T-Matrix Method. (1990). *Light Scattering
by Particles: Computational Methods Advanced Series in Applied Physics,* 79-
185. doi:10.1142/9789814317689_0003

45) Zhao, L., Kelly, K. L., & Schatz, G. C. (2003). The Extinction Spectra of Silver
Nanoparticle Arrays: Influence of Array Structure on Plasmon Resonance
Wavelength and Width†. *The Journal of Physical Chemistry B, 107*(30), 7343-
7350. doi:10.1021/jp034235j

46) Ravi, A., Luthra, A., Teixeira, F. L., Berger, P. R., & Coe, J. V. (2015). Tuning
the Plasmonic Extinction Resonances of Hexagonal Arrays of Ag
Nanoparticles. *Plasmonics, 10*(6), 1505-1512. doi:10.1007/s11468-015-9963-9

47) Zhou, L., Yu, X., & Zhu, Y. (2006). Propagation and dual-localization of surface
plasmon polaritons in a quasiperiodic metal heterowaveguide. *Applied Physics
Letters, 89*(5), 051901. doi:10.1063/1.2236297

48) Venugopal, N., & Mitra, A. (2013). Localized surface plasmon resonance of silver
nanoisland based glucose sensor. doi:10.1063/1.4810669

49) Ge, J., Hu, Y., Biasini, M., Beyermann, W., & Yin, Y. (2007). Superparamagnetic
Magnetite Colloidal Nanocrystal Clusters. *Angewandte Chemie, 119*(23), 4420-
4423. doi:10.1002/ange.200700197

50) Lu, Z., Gao, C., Zhang, Q., Chi, M., Howe, J. Y., & Yin, Y. (2011). Direct
Assembly of Hydrophobic Nanoparticles to Multifunctional Structures. *Nano
Letters, 11*(8), 3404-3412. doi:10.1021/nl201820r

51) Nie, Z., Petukhova, A., & Kumacheva, E. (2009). Properties and emerging
applications of self-assembled structures made from inorganic
nanoparticles. *Nature Nanotechnology, 5*(1), 15-25. doi:10.1038/nnano.2009.453

52) Ge, J., Hu, Y., & Yin, Y. (2007). Highly Tunable Superparamagnetic Colloidal
Photonic Crystals. *Angewandte Chemie International Edition, 46*(39), 7428-7431.
doi:10.1002/anie.200701992

53) Sokolov, K. V. (2014). Plasmonic nanosensors for molecular and functional cancer imaging and therapy (presentation video). *Biosensing and Nanomedicine VII*. doi:10.1117/12.2064743

54) Kar, S., Desmonda, C., & Tai, Y. (2013). Synthesis of SERS-Active Stable Anisotropic Silver Nanostructures Constituted by Self-Assembly of Multiple Silver Nanopetals. *Plasmonics, 9*(3), 485-492. doi:10.1007/s11468-013-9646-3

55) Lin, S., Li, M., Dujardin, E., Girard, C., & Mann, S. (2005). One-Dimensional Plasmon Coupling by Facile Self-Assembly of Gold Nanoparticles into Branched Chain Networks. *Advanced Materials, 17*(21), 2553-2559. doi:10.1002/adma.200500828

56) Zhang, H., & Wang, D. (2008). Controlling the Growth of Charged-Nanoparticle Chains through Interparticle Electrostatic Repulsion. *Angewandte Chemie,120*(21), 4048-4051. doi:10.1002/ange.200705537

57) Choueiri, R. M., Klinkova, A., Thérien-Aubin, H., Rubinstein, M., & Kumacheva, E. (2013). Structural Transitions in Nanoparticle Assemblies Governed by Competing Nanoscale Forces. *Journal of the American Chemical Society, 135*(28), 10262-10265. doi:10.1021/ja404341r